Ana Filipa Alves Rodrigues dos Santos

Bachelor in Micro and Nanotechnologies Engineering

Investigation of VO_2 Metal-to-Insulator Transition for application in memory devices

Dissertation submitted to obtain the degree of Master in
Micro and Nanotechnologies Engineering

Adviser: Dr. Joana Pinto, Professora Auxiliar,
Faculdade de Ciências e Tecnologia da Universidade Nova de Lisboa

Co-adviser: Dr. Jonas Deuermeier, Auxiliary Researcher,
Faculdade de Ciências e Tecnologia da Universidade Nova de Lisboa

Júri:
Presidente: Dr. Rodrigo Ferrão de Paiva Martins
Arguente: Dr. João Pedro Sousa Oliveira
Vogal: Dr. Joana Maria Dória Vaz Pinto Morais Sarmento

FACULDADE DE CIÊNCIAS E TECNOLOGIA
UNIVERSIDADE NOVA DE LISBOA

Investigation of VO_2 Metal-Insulator Transition for application in memory devices

Copyright © Ana Filipa Alves Rodrigues dos Santos, Faculdade de Ciências e Tecnologia, Universidade Nova de Lisboa.

A Faculdade de Ciências e Tecnologia e a Universidade Nova de Lisboa têm o direito, perpétuo e sem limites geográficos, de arquivar e publicar esta dissertação através de exemplares impressos reproduzidos em papel ou de forma digital, ou por qualquer outro meio conhecido ou que venha a ser inventado, e de a divulgar através de repositórios científicos e de admitir a sua cópia e distribuição com objetivos educacionais ou de investigação, não comerciais, desde que seja dado crédito ao autor e editor

Acknowledgments

I would like to thank all the people that have been good to me and helped me through this process. It has been a long and hard ride but here I am, finishing my dissertation work and master's degree, something that I thought would not be possible in my life, due to the circumstances.

Firstly, to my advisor Dr. Joana Pinto that made this possible and always had my back, encouraging me to do better and experiment new things. I cannot thank you enough for your knowledge transfer and you will always have a special place in my heart. To my co-adviser, Dr. Jonas Deuermeier who helped with XPS analysis and thesis format. I am truly sorry for the long e-mails and I hope I am not remembered just by it.

To Dr. Rodrigo Martins and Dr. Elvira Fortunato for allowing me to finish this beautiful, hardworking but crazy engineering course in their facilities. I will always be grateful for all the experiences I had and all the things that I have learned in CENIMAT|i3N and CEMOP.

A special thank you to the team at CENIMAT|i3N that helped and guided me during this period: Alexandra Gonçalves, Sónia Pereira, Rita Branquinho, Tomás Calmeiro, Asal Kiazadeh.

To all the friends I made that kept me sane throughout this journey: Carlos, Tibério, Dan, Moura, Catarina, André, Pedro and to my Núcleo de Nanotecnologia buddies. For all these years, the fun memories, the ideas shared, the craziness in the group chats and works. I know I can be hard to deal with sometimes, but I want you to know that you all were very important to me and if it was not for you, I would have not made it this far. So, thank you from the bottom of my heart for making my life a lot better.

To my godsons and goddaughter: Rui, Carioca, Xavi, Nuno and Nia. Thank you for trusting and believing in me the way you do. I hope we can keep these friendships for many, many years. A special thank you to the lovebirds Rui and Nia for being my best friends through these years.

To my special friends: David, Ana, Sérgio, Calão. Thank you for being my true friends all the way. You made these 5/6 years bearable. Thank you for accepting my crazy schedule and routine and for always being there for me when I needed.

Of course, to my study buddie Sobral and to João, Pedro, Quiri and Artur. Thank you for all the laughs and histories. I will always keep these memories and laugh still.

To my boyfriend Miguel, I cannot thank you enough. All you did for me for the past 7 years will never be thanked enough. You are the most amazing person I know, and I am so lucky that I can have you by my side. For all the help and love you gave me and still do, thank you.

To my beloved family for putting up with me and opening my eyes for life. Without you I would never made this far. Thank you for the efforts, sacrifice, belief and love that you gave me. I believe I am a richer person now and that is all because of you. I cannot thank you enough, too.

A special thanks to my coaches at LX Team, in particular to Vasco and Tomé for always wanting more of me and for making me reach my limits, every day. To Ana, thank you for all the advices and understanding. Thank you for everything, really, and I hope we can potentiate our work for many years.

Last but not least, to Tiago Teixeira. I like to call you my bigger brother just because you took care of me for so long and still do. Always with a smile on your face and with a heart that cannot fill any room. Thank you for every conversation and encouragement. Thank you for being one of the best people I know and for making me into one of them.

Thank you to all the special people in my life.

Abstract

Vanadium oxides have been extensively studied due to their multiple forms. In particular, VO_2 presents a reversible and ultrafast metal-to-insulator transition (MIT) occurring at ~68ºC that changes the material from monoclinic to tetragonal rutile structure. An external input (thermal, chemical or electronic) can trigger this transition, changing it from a high resistance state to a low resistance state, meaning that it can be used as an electronic switch.

In this project, the optimized conditions to produce VO_2 thin films (~200 nm of thickness) were studied and films were deposited by e-beam evaporation and rf magnetron sputtering (with different O_2 pressures), followed by a Rapid Thermal Annealing (RTA) treatment at different temperatures. The structural, chemical, electronic and morphological properties of VO_2 thin films were characterized by means of X-Ray Diffraction (XRD), X-Ray Photoelectron Spectroscopy (XPS) and Atomic Force Microscope (AFM).

E-beam deposited films were not very reproducible due to contaminations of the tungsten crucible and it was difficult to evaporate the VO_2 pellets. The films were amorphous after deposition and the annealing performed shown that VO_2 monoclinic phase was achieved at 500ºC. The substrate used was Glass/ITO. As RTA temperature increased and O_2 pressure decreased, the crystallization and roughness of the films increased.

The optimized conditions for sputtering were attained with $3x10^{-5}$ mbar of O_2 pressure and RTA temperature of 450ºC in a N_2 environment with a base pressure of 250 mbar. MIM devices were fabricated with sputtering where Molibdenium (Mo) metal was on top of VO_2, using shadow masks with circular contacts and using ITO films as the back contact.

An in-situ heating characterization was performed in XRD and XPS to analyze the transition in terms of phase changes as well as chemical and electronic properties. Preliminary electrical characterization was performed to explore the MIT on optimized VO_2 thin films.

Keywords: VO_2(M), Metal-to-Insulator transition, sputtering, XRD, XPS, MIM devices.

Resumo

Os óxidos de vanádio têm sido bastante estudados devido às suas múltiplas formas e fases. Em particular, o VO_2 apresenta uma transição metal-isolante (MIT) reversível e ultrarrápida que ocorre a ~68ºC que altera o material de estrutura monoclínica para tetragonal rutile. Um estímulo externo (térmico, químico ou elétrico) pode provocar esta transição, alterando-a de um estado de alta resistência para baixa resistência, significando que pode ser usado como interruptor elétrico.

Neste trabalho, foram estudadas as condições ótimas para produzir filmes finos de VO_2 (~200 nm de espessura). Foram depositados por e-beam evaporation e rf magnetron sputtering (a diferentes pressões de O_2), seguidos de um tratamento RTA a diferentes temperaturas. A composição estrutural dos filmes finos de VO_2 foi caracterizada por XRD, XPS e AFM.

Os filmes depositados por e-beam não são reproduzíveis devido a contaminações do cadinho de tungsténio e foi difícil evaporar os “pellets” de VO2. Os filmes eram amorfos depois da deposição e o recozimento realizado mostrou que a fase monoclínica de VO2 foi atingida com sucesso a 500ºC. O substrato utilizado foi Vidro/ITO. À medida que a temperatura aumentava e a pressão de O_2 diminuía, a cristalização e rugosidade dos filmes aumentava.

As condições ótimas por sputtering foi obtida para $3x10^{-5}$ mbar de pressão de O_2 e temperatura de 450ºC num ambiente de N_2 com uma pressão base de 250 mbar. Dispositivos MIM foram fabricados por sputtering onde Molibdénio (Mo) foi o metal depositado por cima do VO_2, usando máscaras com contactos circulares e usando filmes de ITO como contacto de baixo.

A caracterização in-situ com aquecimento foi realizada no XRD e XPS para se analisar a transição in termos de diferenças de fase assim como as propriedades químicas e elétricas. A caracterização elétrica preliminar foi realizada para explorar a MIT em filmes finos de VO_2 otimizados.

Palavras-chave: VO_2 (M), transição metal-isolante, sputtering, XRD, XPS, dispositivos MIM.

Table of Contents

Acknowledgments ... i
Abstract ... iii
Resumo ... v
Table of Contents ... vii
List of Figures ... ix
List of Tables ... xi
List of Acronyms and Abbreviations ... xiii
List of Symbols ... iii
Motivation ... v
Objectives ... vii
1. Introduction ... 1
1.1 XPS measurements ... 4
2. Materials and Methods ... 7
2.1 Vanadium oxides deposition ... 7
2.2 Rapid Thermal Annealing (RTA) ... 7
2.3 Metal contacts deposition ... 8
2.4 X-Ray Diffraction (XRD) measurements ... 8
2.5 X-Ray Photoelectron Spectroscopy (XPS) measurements ... 8
2.6 Atomic Force Microscope measurements ... 9
2.7 Electrical characterization ... 9
3. Results and Discussion ... 11
3.1 Vanadium oxides produced by e-beam evaporation ... 11
3.1.1 X-Ray Diffraction (XRD) ... 11
3.1.2 X-Ray Photoelectron Spectroscopy (XPS) ... 12
3.1.3 Atomic Force Microscopy (AFM) ... 13
3.2 Vanadium oxides produced by RF Magnetron Sputtering ... 14
3.2.1 X-Ray Diffraction (XRD) ... 15
3.2.2 X-ray Photoelectron Spectroscopy (XPS) ... 18
3.2.3 Atomic Force Microscopy (AFM) ... 22
3.3 In-situ measurements in MIM VO_2 devices ... 23
3.3.1 XRD in-situ ... 24
3.3.2 In-situ heating experiments in the XPS chamber ... 24
3.3.3 Electrical Characterization of MIM devices ... 29
4. Conclusion and Future Perspectives ... 33
5. Bibliography ... 35
6. Annexes ... 37
Annex A – AFM measurements ... 37
Annex B – Thin films resistors designs ... 39
Annex C – ITO characterization with thin film resistors ... 40

List of Figures

Figure 1 - Schematic of VO_2 reversible metal-to-insulator transition v
Figure 2 - VO_2 MIT transition: structure change from a) monoclinic phase to b) tetragonal rutile phase and band structure 2
Figure 3 - Utilizing MIT as a switch from the OFF state (high resistance) to the ON state (low resistance) [6] 3
Figure 4 - Applications of the ultrafast oxide MIT [6] 4
Figure 5 - Representation of XPS spectra with VO_2 powder pellets with a V_2O_5 reference [11] 5
Figure 6 - Representations of XPS analysis of different vanadium oxides: a) [12]; b) [10] 6
Figure 7 - Schematic of deposition procedure 8
Figure 8 - XRD scans of e-beam samples 11
Figure 9 - XPS spectra of sputtered VO_x thin films: a) full spectrum; b) oxidation state contributions 12
Figure 10 - Results of e-beam samples by AFM analysis: a) RT; b) 300ºC; c) 400ºC; d) 450ºC; e) 500ºC 14
Figure 11 - XRD scans of all sputtered thin films 15
Figure 12 - XRD scans of D1 group samples 16
Figure 13 - XRD scans of D2 group samples 17
Figure 14 - XRD scans of D3 group samples 17
Figure 15 - XPS spectra of D1 group samples: a) all spectra; b) oxidation state peaks contributions 18
Figure 16 - XPS spectra of D2 group samples: a) all samples; b) oxidation state contributions 20
Figure 17 - XPS spectra of D3 group samples: a) all spectra; b) oxidation state contributions 21
Figure 18 - AFM 3D representation of D1 group sample surfaces: a) D1_RT; b) D1_400; c) D1_450; d) D1_500 22
Figure 19 - AFM 3D representation of the samples annealed at 450ºC 23
Figure 20 - XRD scans of VO_2 thin films with temperature ramps 24
Figure 21 - XRD spectra of optimized VO_2 thin films with increasing temperature: a) all spectra; b) oxidation state contributions 25
Figure 22 - Representation of VO2 thin films valence band with increased temperature 26
Figure 23 - XRD spectrum of optimized VO2 thin films with decreasing temperature: a) all spectra; b) oxidation state contributions 27
Figure 24 - Representation of VO_2 thin film valence band with decreased temperature 28
Figure 25 - XPS spectrum of VO_2 thin film kept in the vacuum chamber for four days: a) all spectra; b) oxidation state contributions 29
Figure 26 - Electrical characterization of VO2 thin film MIM devices 30
Figure 27 - Electrical characterization of VO2 thin film MIM devices with increased temperature 31
Figure 28 - Resistance evolution of VO2 thin film MIM devices with increased temperature 31

Figure 29 - AFM 3D representations of D2 group samples: a) D2_RT; b) D2_400; c) D2_450; d) D2_500 37
Figure 30 - AFM 3D representations of D3 group samples: a) D3_RT; b) D3_400; c) D3_450; d) D3_500 38
Figure 31 - Thin films resistor designs with different width between stripes 39
Figure 32 - IV curves representation of a test using a resistor design as a possible heating element 40

List of Tables

Table 1 - The crystallography data of some important types of VO_2 polymorph................1
Table 2 - Sample names according to deposition and annealing conditions......................7
Table 3 - Parameters of XPS for e-beam samples 13
Table 4 - AFM parameters of e-beam samples 14
Table 5 - XPS parameters of D1 group samples 19
Table 6 - XPS parameters of D2 group samples 20
Table 7 - XPS parameters of D3 group samples 21
Table 8 - Structural parameters extracted from AFM for D1 group samples 22
Table 9 - Structural parameters extracted from AFM for the samples annealed at 450ºC23
Table 10 - XPS parameters of optimized VO_2 thin films with increasing temperature 25
Table 11 - XPS parameters of VO_2 thin films with decreased temperature 27
Table 12 - Structural parameters extracted from AFM for the D2 group samples 37
Table 13 - Structural parameters extracted from AFM for the D3 group samples 38

List of Acronyms and Abbreviations

AFM	Atomic Force Microscopy
CENIMAT|i3N	Centro de Investigação de Materiais | Instituto de Nanoestruturas, Nanomodelação e Nanofabricação
CEMOP	Centro de Excelência de Microeletrónica, Optoeletrónica e Processos
CCD	Charged Coupled Device
CVD	Chemical Vapor Deposition
DRAM	Dynamic Random-Access Memory
ISCD	Inorganic Crystal Structure
ITO	Indium Tin Oxide
MIT	Metal-to-Insulator Transition
PVD	Physical Vapor Deposition
RMS	Root mean square
RT	Room Temperature
RTA	Rapid Thermal Annealing
TCO	Transparent Conducting Film
UHV	Ultra-High Vacuum
XPS	X-ray Photoelectron Spectroscopy
XRD	X-Ray Diffraction

List of Symbols

A/s	Ampere per second
BE	Binding Energy
FWHM	Full Width at Half Maximum
I	Current
R	Resistance
ρ	Resistivity
T	Temperature
VB	Valence Band

Motivation

"Consumers have come to expect increasingly sophisticated electronics products at ever lower prices, just as the business world has come to expect greater productivity through improved information technology." *Chris A. Mack* on "Fifty years of Moore's law" [1]. The demand for new technologies with faster response, higher density, lower power consumption is taking engineering to a whole other level and, referring to Moore's law, there are some questions concerning its future.

Moore's law has survived half a century always adjusting its prediction, travelling from CCD, DRAM, Flash memories, among others [1]. It is thought to be reaching its saturation point due to physical limits of scalability from the elements composing these memory devices.

One of the most promising memory devices is called memristor or memory resistor. This device was theoretically found by *L.Chua* in 1971 and was predicted to be the "missing" element in circuitry [2]. This device is also a passive element, but its function cannot be compared with a resistor, capacitor or inductor. These types of devices can have multiple resistance states regarding their physical composition [3].

Materials with a metal-to-insulator transition (MIT) are some of the best fit for these types of electronics according to their resistive switching and fast response. VO_2 is one of the most fascinating materials since it is known by an ultrafast (picoseconds) and reversible phase transition [3]–[7].

One more advantage of VO_2 is that the MIT can occur near room temperature since its transition occurs around 68ºC (341K). This transition can change its resistance value by several orders of magnitude and also, its structure. Below transition temperature, VO_2 behaves as a semiconductor (monoclinic structure) with a high resistance state. Above transition temperature, VO_2 behaves as a metal (tetragonal rutile structure) with a low resistance state [5], [6], [8].

In Figure 1, a schematic of this transition and the structural change is represented.

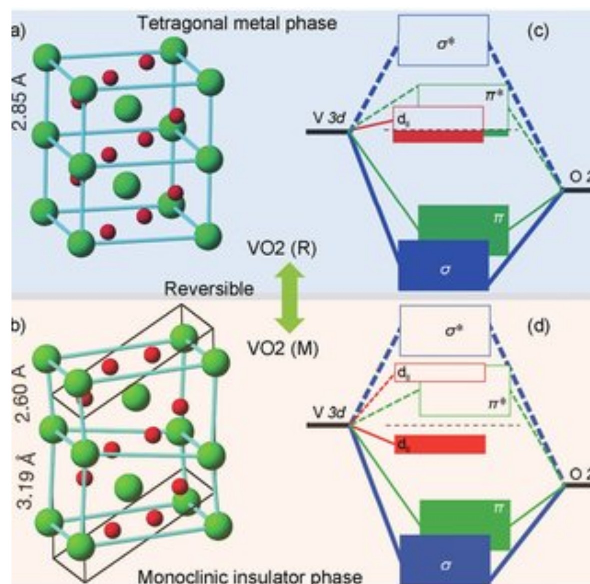

Figure 1 - Schematic of VO_2 reversible metal-to-insulator transition

Objectives

In this project, the intention is to explore the VO_2 metal to insulator transition and for that, it is essential to know about its synthesis and properties. The ultimate goal is the analysis of the structural, electrical and optical properties of VO_2 thin films in order to conclude their use for memory devices.

This goal is divided in five essential parts:

1. Deposition of VO_2 thin film by e-beam evaporation and RF Sputtering, followed by RTA treatment at different temperatures.
2. Characterization and comparison of the films by XRD, XPS and AFM.
3. Fabrication of MIM devices with the optimized conditions of the VO_2 thin films produced by RF Sputtering.
4. Electrical characterization and in-situ characterization with XRD and XPS of MIM devices.

1. Introduction

The vanadium oxides are in continuous study in multiple forms, since they can be used in various applications. The main reason for this is the different valences they can provide such as, V_2O_5, V_2O_3 VO_2 and VO. According to *Surnev et.al*, the vanadium oxides interest is centred around their phase transition [9]. In this project, the intention is to explore the VO_2 metal-to-insulator (MIT) transition and to optimize its synthesis conditions and properties.

For its synthesis, VO_2 has been tested in multiple forms as bulk single crystal, thin films in both epitaxial and polycrystalline forms and different nanostructures. For the growth of the VO_2 thin films, different methods have been used such as CVD (Chemical Vapor Deposition), PVD (Physical Vapor Deposition), e-beam evaporation (electron-beam evaporation), rf magnetron sputtering (radio frequency magnetron sputtering), among others [6].

As is well known, vanadium can have several oxidation states that can go from 0 to +5. These oxidation state correspond to different vanadium oxides, for example +4 corresponds to VO_2 and +5 can correspond to V_2O_5 or V_6O_{13} [10]–[12]. VO_2 is also know by having a variety of polymorphs and in Table 1 are represented the ones found or referred to in this dissertation.

Table 1 - The crystallography data of some important types of VO_2 polymorph (Adapted from [13]*)*

Phase	**T_c (ºC)**	**Crystal system (Cs)**	**Space group (Sg)**	**a [Å]**	**b [Å]**	**c [Å]**	**Ref.**
VO_2 (B)	-	Monoclinic	C2/m	12.03	3.69	6.42	[13]
VO_2 (M)	68ºC	Monoclinic	P21/c	5.74	4.16	5.38	[13]
VO_2 (R)	68ºC	Tetragonal	P42/mnm	4.53	4.53	2.87	[13]

In the table above can be seen the MIT at 68ºC, referred earlier as transition temperature (T_c), for the monoclinic phase (VO_2 (M)) and for the tetragonal phase (VO_2 (R)). Also, a commonly found monoclinic phase is shown (VO_2 (B)) but this one doesn't show a transition temperature and is normally researched as a cathode material for Li-on batteries [14].

Even though this project consists in using VO_2 thin films for electrical switching devices, li-on batteries, as mentioned, and thermochromic applications for this material are already being studied [13], [15]. For these applications, colloidal and hydrothermal synthesis methods are commonly used.

According to *Yang et al.*, there are some elementary mechanisms of the MIT which consider the interactions occurring in the insulator. For an example, if there are electron-electron interactions in the insulator, the MIT is called Mott-Hubbard MIT. Although, the interactions between electrons and the lattice cannot be forgotten and so, the interactions between electrons and phonons (which are the vibrations of the lattice) are called Peierls MIT. This transition is caused by a structure change which induces a lattice deformation and later, results in a band structure change. Anderson MIT is based on the disordered electron localizations in the lattice, which is more common in heavily doped semiconductors. Finally, there is a band insulator or Bloch-Wilson insulator which doesn't considerate the electron-electron interactions such as diamonds or undoped semiconductors [6].

The elementary mechanisms of MIT must be controlled and there are three different types, which can be: Temperature control, bandwidth control and band-filling control. The first one, as

its name says only involves changes by heating or cooling. The bandwidth control is related to the external or internal pressure. The last one, is focusing on tuning the doping level with donors or acceptors [6].

There is some discordance and doubts about which MIT transition VO_2 might be, since there is no clear definition with the interactions. Some say it is Mott-Hubbard, others say it is Peierls [6], [16].

Vanadium dioxide (VO_2) is a material that, when is heated near 70°C (more precisely at 68°C), has a transition from the metal phase to the insulator phase (MIT), changing from a monoclinic structure to a tetragonal rutile structure. Changing the structure is related to the valence and conduction bands of the materials since below the MIT the material behaves as a semiconductor having a gap between bands and above the MIT functions as a metal (no gap between bands). This way, in Figure 2, the MIT is represented [6], [7], [17].

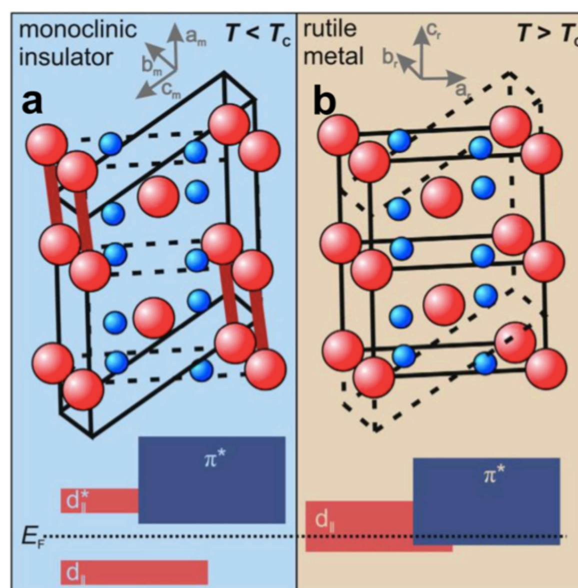

Figure 2 - VO_2 MIT transition: structure change from a) monoclinic phase to b) tetragonal rutile phase and band structure [17]

As it is shown in Figure 3, the materials with the MIT can work as a switch. An external input can trigger this transition, changing from the OFF state (high resistance) to an ON state (low resistance). For VO_2 thin films, this change occurs from 67ºC to 71ºC. This property gives a useful guideline for resistive memory switching devices (known as memristors) because it is known by being ultrafast and reversible [3]–[7].

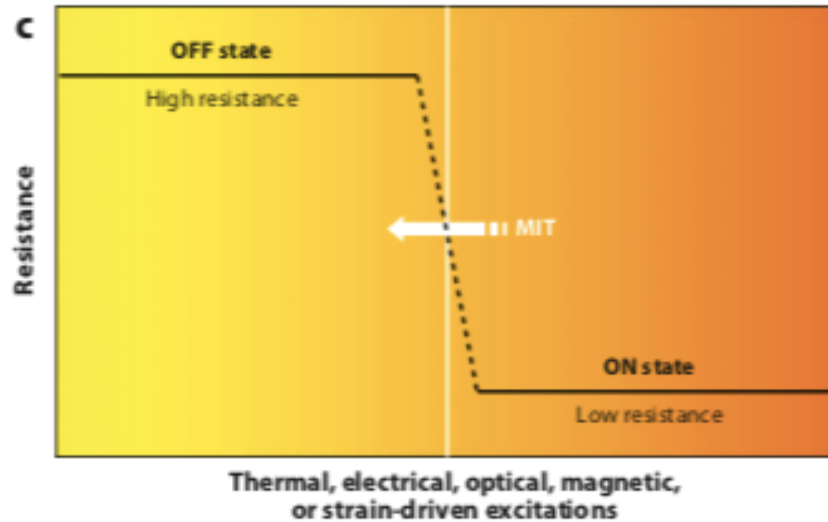

Figure 3 - Utilizing MIT as a switch from the OFF state (high resistance) to the ON state (low resistance) [6]

The structure of the memristor consists on an oxide material embedded between two metal contacts, which is called MIM (metal-insulator-metal) structure and which can be electrically switched between two or more states. These devices have different mechanisms according to the external input, which can be thermal, chemical or electronic [2], [18], [19].

A memristor is an electrical component that limits or regulates the flow of the current in the device and remembers this one like a memory. These devices are nonlinear, and, more importantly, non-volatile, which means that they can retain memory without a power source. This also means that when a current is flowing through the device, a resistance is retained. Therefore, in order to learn more about the memristor properties during the MIT, the resistance can be measured by resistance states, hysteresis in heating or cooling the substrate, among others [20].

The characterization of these devices consists in measuring the I-V curves which can show the change in the structure of VO_2 and the resistance associated with this phenomenon.

As it is seen in Figure 4, there are some applications for the MIT such as memristive elements, metamaterials, thermal and chemical sensors, etc.

Figure 4 - Applications of the ultrafast oxide MIT [6]

There are a lot of studies around VO_2 and these resistive memory switching devices can have different structures as well as three-terminal gated field effect switches and metal-insulator transition oscillators [6].

Finally, the MIM devices with VO_2 thin films will also be characterized by XRD (X-Ray Diffraction) and XPS (X-Ray Photoelectron Spectroscopy) in-situ. Also, an electrical characterization will be carried out.

1.1 XPS measurements

As mentioned before, vanadium oxides can have multiple forms and structures [10]–[12]. With the XPS analysis, the attempt is to find those forms in order to distinguish them according to their oxidation state. Furthermore, the technique is used to study MIT-induced changes to the electronic density of states at the Fermi level.

The oxidation state, as said earlier, can go from 0 to +5 and in this work, more attention was given to V^{4+} and V^{5+} since, they correspond to VO_2 and V_2O_5, respectively. Many intermediate oxidation states are present in vanadium oxides with different stoichiometry such as V_6O_{13} that can also represent V^{5+} [10]–[12].

To better understand the oxidation state, in Figure 5, there are represented three samples from *Silversmit et al*. where V^{4+} and V^{5+} are represented. The O 1s peak is also represented with the contaminations that can appear. The VO_2 (AA or SA) presented in the figure below only differ in the supplier of the powders.

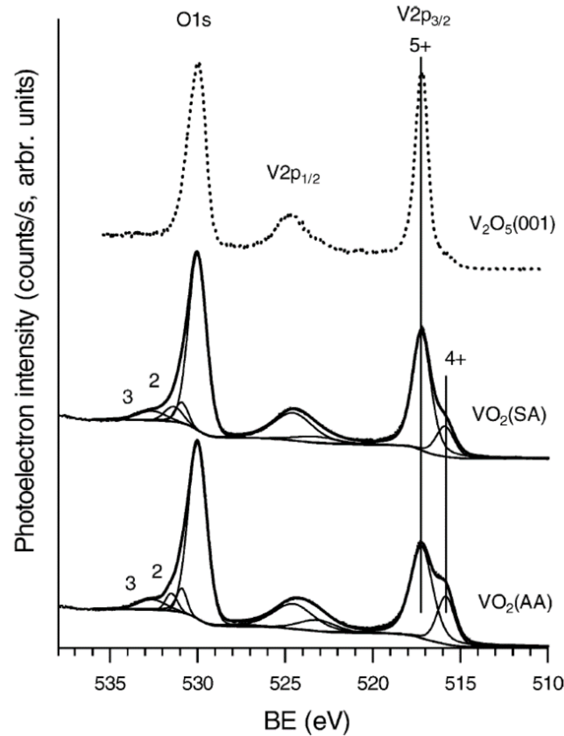

Figure 5 - Representation of XPS spectra with VO_2 powder pellets with a V_2O_5 reference [11]

V 2p and O 1s are represented in Figure 5. V 2p is divided in two peaks (V $2p_{3/2}$ and V $2p_{1/2}$) and to analyze the oxidation state peaks, only V $2p_{3/2}$ is considered. As seen, the V^{4+} and V^{5+} are demonstrated and change according to the VO_x form. It is important to check the V^{4+}/V^{5+} ratio present in every sample in order to confirm the VO_x form. These can change due to the deposition conditions of the samples or even the RTA temperature [10]–[12].

Concerning the O 1s peak, numbers 2 and 3 relate to OH^- and H_2O contaminations, respectively. These can come from long exposure to air or adsorbed water which can induce over-oxidation on the samples surface. One more contribution for this can be the O_2 pressure used since it varies in sputtering depositions. Over-oxidation can also be seen with the widening of the peaks and the increase of intensity in V $2p_{3/2}$ and V $2p_{1/2}$ [11].

In Figure 6, two more examples of these spectra forms are represented in order to simplify the analysis. In Figure 6 a), only the V 2p peak is represented and the oxidation of the samples related to increased intensity of V 2p peak, clearly in V $2p_{1/2}$, can be seen. To better understand the differences between V_2O_5 and V_6O_{13}, Figure 6 b) from *Mendialdua et al.* is shown.

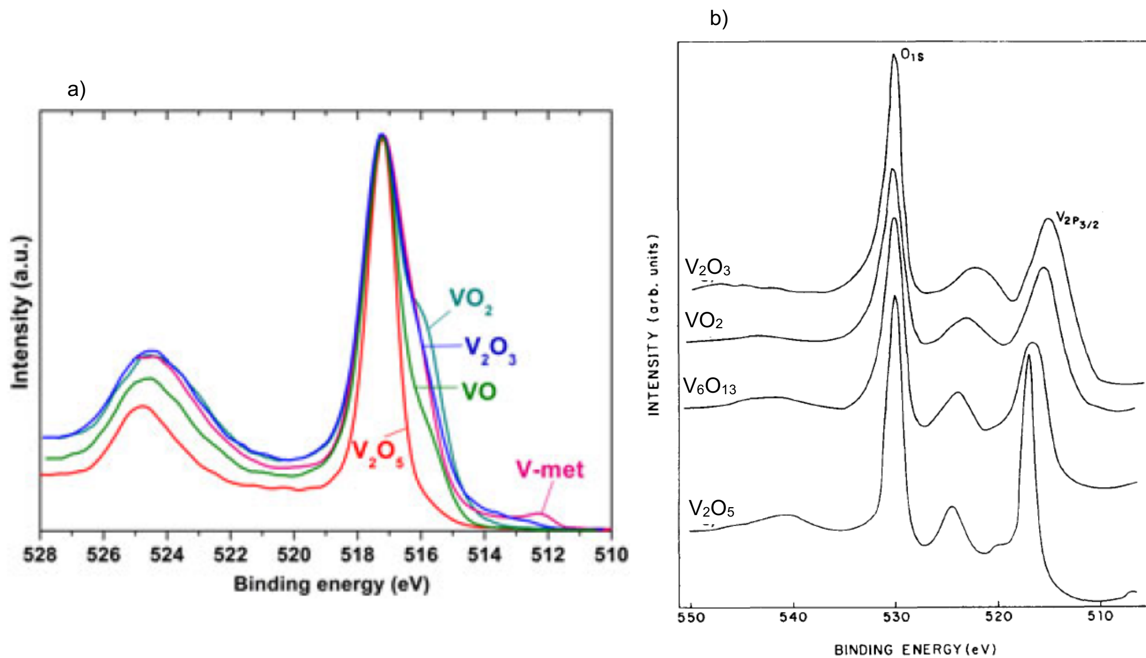

Figure 6 - Representations of XPS analysis of different vanadium oxides: a) [12]*; b)* [10]

In Figure 6 a), V_2O_5 and VO_2 are expressed which correspond to V^{5+} and V^{4+} oxidation state. Then, VO and V-met are also represented and relate to V^{2+} and $V^{(0)}$. V-met corresponds to the metallic state. These are the spectra to look for and there are some differences according to binding energy (BE) and, the shape of the peak. V_2O_5 is known by the straight peak and VO_2 has a ledge between 515-516 eV. V_2O_3 relates to the V^{3+} peak and does not show the ledge that VO_2 shows. The difference between V_2O_3 and VO_2 is that VO_2 creates this ledge and V_2O_3 widens the peak since V^{3+} is located to the right of the V^{4+} peak [10]–[12].

As said before, V^{5+} can relate to V_2O_5 or V_6O_{13} but the big difference between them is the straight peaks of V_2O_5 which is observed when in comparison with other samples [10]. This relates to the Full Width at Half Maximum (FWHM) meaning that when this value is higher, the wider the peak is and when it is lower, the narrower it is. This widening and narrowing of the peaks can correspond to different vanadium oxides as for example, the narrowest peaks are V_2O_5.

To help this analysis, Binding Energy (BE) values, Full Width at Half Maximum (FWHM) of the peaks, V^{4+}/V^{5+} content and V/O ratio present in *CasaXPS* software were taken in consideration.

Finally, it is important to say that this analysis only corresponds to the first 5-10 nm of the sample surface.

2. Materials and Methods

To produce VO_2 thin films of ~200 nm, depositions were carried with e-beam evaporation and rf magnetron sputtering. The films were deposited on Corning Glass coated with ITO.

There were two sample configurations prepared: In the first one, the VO_2 film was deposited directly on the ITO film where ITO serves as the bottom contact in MIM devices; for the other one, the VO_2 film is deposited on the face directly on glass and ITO (deposited on the back face) serves as a possible heating resistive element. Then, the condition where VO_2 monoclinic phase appeared, was reproduced to perform in-situ experiments in both XRD and XPS techniques.

2.1 Vanadium oxides deposition

Two different Physical Vapor Deposition (PVD) techniques were used to produce vanadium oxides thin films: electron beam assisted evaporation (e-beam) and magnetron rf sputtering, both in CEMOP Clean Room.

E-beam evaporation was performed in a home-made system (*Orient express*), using VO_2 pellets with 99.99% purity as the evaporation material and using a tungsten crucible. The depositions were performed in vacuum, ensuring an initial vacuum pressure below $5x10^{-6}$ mbar. The thickness of the films was controlled using a quartz thickness monitor. All depositions were performed at 6 kV using a high voltage module, with currents that varied between 5 to 20 mA, and growth rates varying from 0.2 to 3 A/s.

Sputtering films were produced in a home-made sputtering system (*3 Target*) using a V sputtering target of 2" diameter from Alineason with 99.999% purity. Three different O_2 partial pressures were tested during this work ($1x10^{-5}$ mbar, $3x10^{-5}$ mbar, $5x10^{-5}$ mbar) and the deposition pressure was kept constant at $1.5x10^{-3}$ mbar ($p_{Ar} + p_{O2}$).

2.2 Rapid Thermal Annealing (RTA)

The samples were annealed with a Rapid Thermal Annealing system (RTA in AS-One RTP System) at different temperatures: 300°C, 400°C, 450°C and 500°C. This procedure was under 250 mbar of N_2 atmosphere with a holding time of 300 s and using a heating rate of 50°C/s, which allowed the crystallization of the oxide. The heating and cooling time were controlled by the system and are the fastest possible. The cooling time was around 10 min. Table 2 shows the name of the samples used according to deposition and temperature.

Table 2 - Sample names according to deposition and annealing conditions

		Sputtering (mbar)		
Temperature (ºC)	**E-beam**	$5x10^{-5}$	$3x10^{-5}$	$1x10^{-5}$
RT	C_RT	D1_RT	D2_RT	D3_RT
300	C_300	-	-	-
400	C_400	D1_400	D2_400	D3_400
450	C_450	D1_450	D2_450	D3_450
500	C_500	D1_500	D2_500	D3_500

These set of conditions were chosen following a previous work performed at CENIMAT on e-beam deposited thin films [21].

2.3 Metal contacts deposition

Metal contacts were deposit after RTA treatment by RF-Sputtering with Molybdenum (Mo) at RT.

An aluminum shadow mask was used to pattern circular contacts of 1 mm diameter for the MIM devices and striped contacts for in-plane devices.

Figure 7 shows a schematic of the deposition procedure for the sample configurations studied in this work.

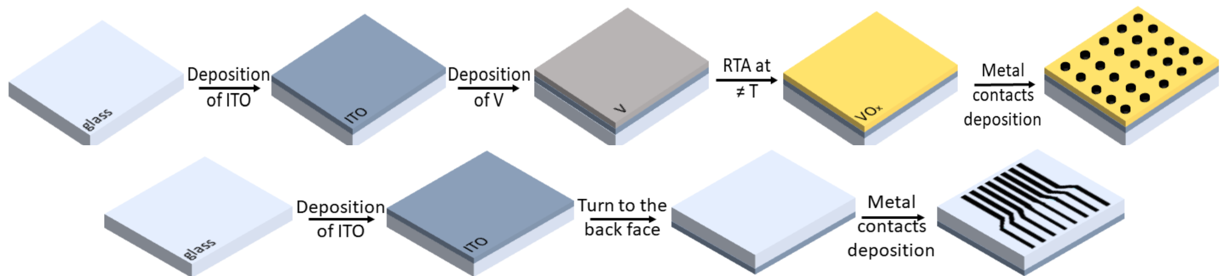

Figure 7 - Schematic of deposition procedure

In order to produce heating elements on the back face of the samples, thin film resistor masks were draw in Adobe Illustrator to patterned conductive thin films. These designs are presented on Annex for reference.

2.4 X-Ray Diffraction (XRD) measurements

The XRD measurements were performed in PANalyticalX'Pert Pro X-Ray diffractometer, equipped with an X'Celerator 1D detector and using CuK_α radiation. The XRD data were obtained in the Bragg-Brentano configuration, with a step size of 0.02º 2θ, in a range of 2θ between 15º to 90º. For phase identifications, the scans were compared to the standard patterns from the Inorganic Crystal Structure Database (ICSD) shown in annexes.

2.5 X-Ray Photoelectron Spectroscopy (XPS) measurements

The XPS measurements were performed in a Kratos Axis Supra spectrometer. All detail spectra were recorded with a pass energy of 10 eV. The data analysis was performed with *CasaXPS* software version 2.3.19PR1.0. A Shirley function was used to subtract the background. The O 1s and V 2p peaks were fitted with Gaussian-Lorentz (GL(30)) curves, meaning 30% corresponds to the Lorentzian profile and 70% to the Gaussian profile. *Biesinger et al.* said "The best mixture of Gaussian-Lorentzian components will vary depending on the instrument and resolution (pass energy) settings used as well as on the natural line-width of the specific core hole". As the O 1s line has a larger natural line-width, this profile curve is the best fit. All samples were charge-corrected by O 1s peak at 530 eV [22]. The only exception is the valence band (VB)

of the samples where temperature ramps were applied. Here, the Fermi edge was calibrated to a binding energy of 0 eV.

2.6 Atomic Force Microscope measurements

The AFM measurements were performed in an MFP-3D AFM system from Asylum in tapping mode and using an Olympus AC160TS tip (K = 26 N/m; F_0 = 300 kHz). In each sample, an area of 5 µm by 5 µm was subject to different scans for several times in order to allow the roughness determination.

2.7 Electrical characterization

The electrical characterization of the films was performed on an Agilent 4155C semiconductor parameter analyzer using a Cascade Microtech M150 manual microprobe in order to confirm the electrical change. For that, I-V measurements were performed using *EasyExpert* software. To analyze the reversible metal-to-insulator transition and using a heating stage of the equipment at different temperatures, IV curves and resistance changes were obtained.

3. Results and Discussion

In this section, the characterization results of all samples are presented. The techniques used were XRD, XPS and AFM. Firstly, deposited films from e-beam were analyzed and some conclusions were made to allow a starting point for sputter deposited films. Afterwards, it was selected the best condition between sputtering samples in order to evaluate the behavior with temperature changes.

It is important to note that these characterization techniques were performed in different days and also with different gaps of days between them which can interfere in the results.

3.1 Vanadium oxides produced by e-beam evaporation

As already presented in Materials and Methods, VO_2 amorphous films were produced by e-beam evaporation and exposed to RTA treatment under N_2 atmosphere at five different temperatures being 300ºC, 400ºC, 450ºC and 500ºC. Films with ~200 nm of thickness were deposited and named hereafter by C_RT to C_500.

3.1.1 X-Ray Diffraction (XRD)

XRD was used primarily to confirm the presence of VO_2 monoclinic phase (VO_2 (M)) or the presence of other phases that could appear due to the annealing temperature. Previous work showed that RTA under N_2 atmosphere is needed to crystallize the thin films into VO_2 (M) and to prevent the formation of other vanadium oxide phases [21].

In Figure 8, XRD scans for e-beam samples annealed at different temperatures are presented.

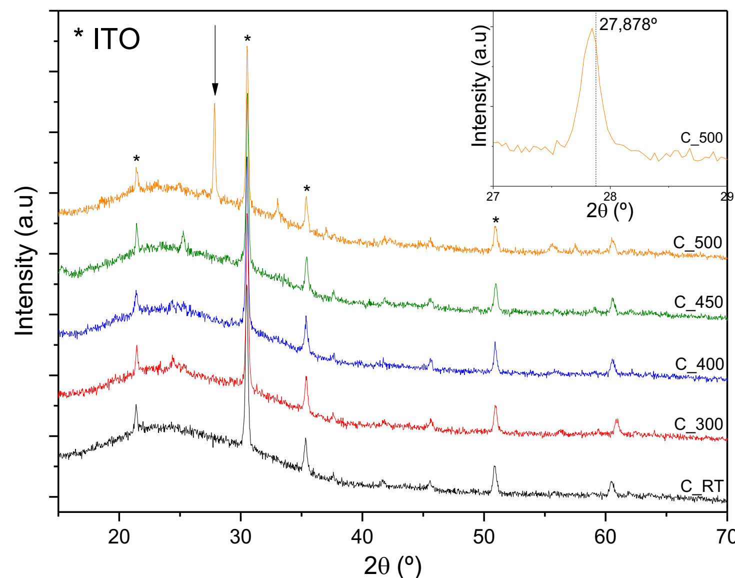

Figure 8 - XRD scans of e-beam samples

As can be seen, all samples have the same peak distribution except for C_500. Only for the latter sample, a peak at 27.878º (~27.9º) is visible and it corresponds to the (011) orientation of VO_2 monoclinic phase with space group P21/c (ISCD #01-072-0514). This peak shows the desirable phase for the metal-to-insulator transition and is the one that is targeted for the sputter depositions.

The other common peaks are related to the ITO, or In_2O_3 orthorhombic structure (ICSD #41-1445) used which was below the VO_x deposited film.

As can be seen, there are some peaks with no label, and these can relate to a mixed phase of vanadium oxide or even other compound that was not identified.

3.1.2 X-Ray Photoelectron Spectroscopy (XPS)

The V 2p and O 1s XPS spectra of VO_2 thin films produced by e-beam are represented in Figure 9 a). As can be seen, different peaks appear, which relate to Vanadium (V 2p) and Oxygen (O 1s).

The core analysis is related to the V $2p_{3/2}$ peak since the oxidation state peaks are the ones used to distinguish which VO_x form is present. In order to make the analysis clearer, a spectrum of all samples was displayed to evaluate the oxygen contributions and contaminations of the samples.

Figure 9 b) corresponds to the oxidation states contributions seen in the V $2p_{3/2}$ peak.

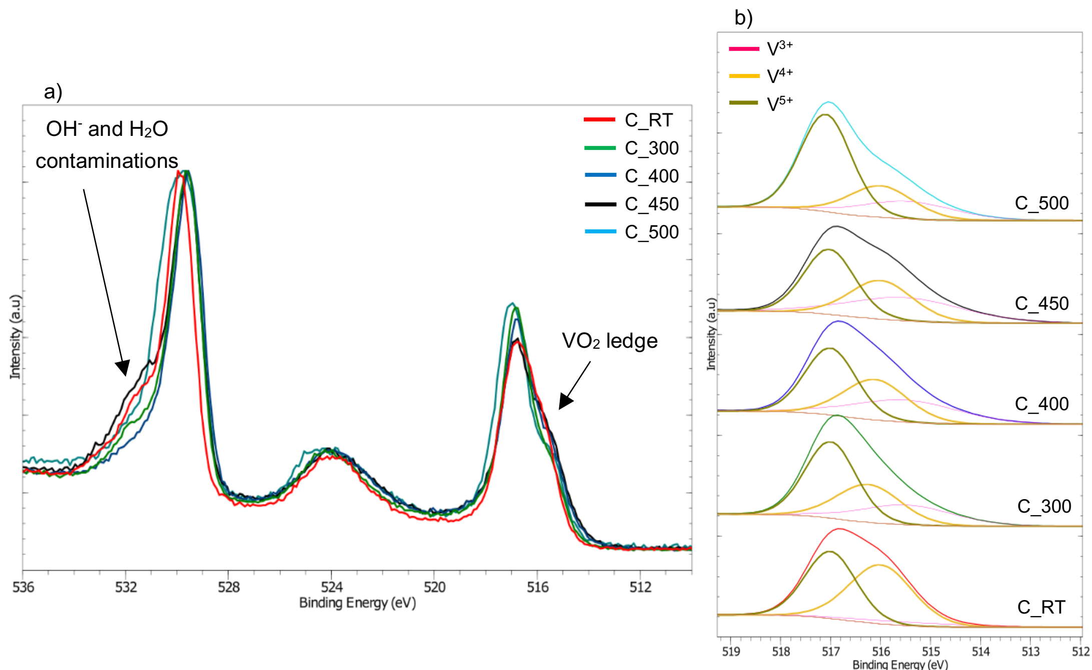

Figure 9 - XPS spectra of sputtered VO_x thin films: a) full spectrum; b) oxidation state contributions

As temperature rises, the V $2p_{3/2}$ peak is narrowing to form the ledge (highlighted by an arrow in Figure 9 a) known in the VO_2 form. Looking at O 1s peak, there are contaminations from C_300 to C_450. This can mean there was over-oxidation at the surface into V_6O_{13}, since V 2p increased its intensity.

The values extracted from *CasaXPS* should be taken in consideration in order to have a more precise analysis, which are presented in Table 3.

Table 3 - Parameters of XPS for e-beam samples

Sample	V^{4+}/ V^{5+}	V/O	$FWHM_{V^{4+}}$	$BE_{V^{4+}}$ (eV)	$FWHM_{V^{5+}}$	$BE_{V^{5+}}$ (eV)
C_RT	1.10	0.38	1.50	516.0	1.20	517.0
C_300	0.62	0.41	1.50	516.2	1.20	517.0
C_400	0.75	0.44	1.50	516.1	1.20	517.0
C_450	0.74	0.37	1.50	516.0	1.20	517.0
C_500	0.40	0.38	1.50	516.0	1.20	517.1

C_RT corresponds to the room temperature sample and it was the only one where V^{4+} peak has a higher percentage than V^{5+}. This can mean that, using e-beam evaporation, VO_2 was already formed with no need for annealing treatment.

From Table 3, C_300 to C_500 showed that the V^{5+} peak is higher than the V^{4+} peak, as already seen in Figure 9 b), since V^{4+}/V^{5+} ratio was inferior to one. This can mean that VO_2 form is no longer present, at the surface. This can be due to the RTA treatment or only to the presence of contaminations in the sample surface that can over-oxidize it. The presence of contaminations can relate to V/O ratio where the oxidations are explicit. As long as oxygen ration increases, oxidation increases, and V/O ratio is lower than 1.

C_500 is the sample where the V^{4+}/V^{5+} ratio was lower indicating that V^{5+} peak increased while V^{4+} peak decreased. This can suggest the formation of V_6O_{13}.

In Figure 9 b), V^{3+} contribution is also showing but since it relates to V_2O_3 and is always lower than V_{4+} and V_{5+} peaks, it wasn't considered for the analysis of VO_x form. However, this contribution can be taking some percentage out of the other two.

It is important to refer that only the first 5-10 nm are being analyzed. Combining both structural techniques, it is possible to conclude that the films only present the monoclinic crystalline structure in bulk after annealing at 500ºC.

Different oxidations states are present in the first nm of the films, even the correct stoichiometry of VO_2. However, a decrease of V^{4+} contribution with the increased annealing temperature confirms the tendency for the film oxidation at the surface [10]. The monoclinic structure is preserved if the bulk is considered.

3.1.3 Atomic Force Microscopy (AFM)

AFM analysis was performed to characterize the surface topography and roughness of the deposited films. This set of samples were produced by e-beam evaporation and were subject to RTA at different temperatures between 300ºC to 500ºC.

In Figure 10 the set of samples is displayed and in Table 4 the parameters that were analyzed.

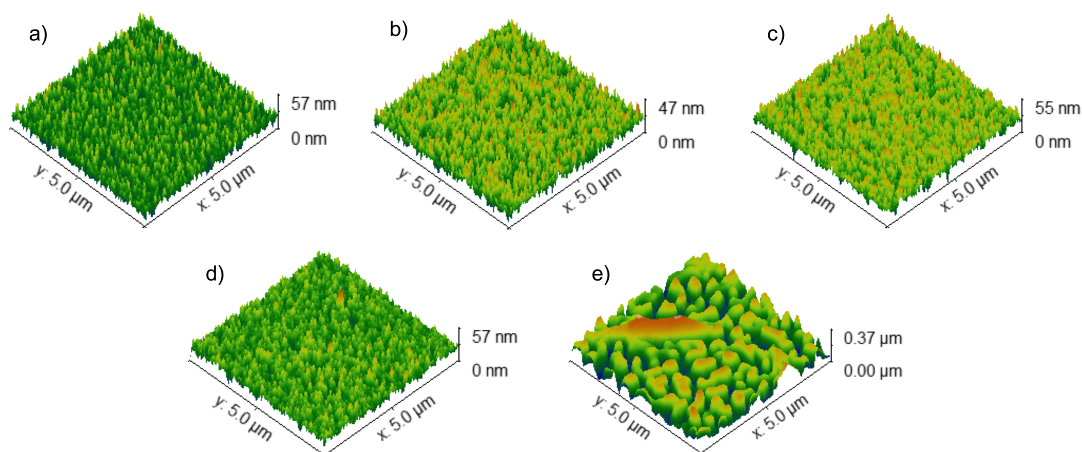

Figure 10 - Results of e-beam samples by AFM analysis: a) RT; b) 300ºC; c) 400ºC; d) 450ºC; e) 500ºC

Table 4 - AFM parameters of e-beam samples

Sample	**RMS Roughness, Sq (nm)**	**Median peak height (nm)**
C_RT	6.0394	19.457
C_300	5.7591	20.503
C_400	5.9457	26.034
C_450	5.0861	23.635
C_500	71.143	173.21

As seen in the figure and table above, the root mean square roughness (Sq) of the samples from C_RT to C_450 are around 5/6 nm. The median peak height between those samples is also similar (~20/25 nm).

C_500 shown an abrupt increase of both parameters which can mean that from 500ºC, the crystallization of the films increases significantly with higher temperatures and Sq and peak height go along.

The annealing temperature of 500ºC was the only one that led to the formation of VO_2 (M), as shown in XRD. With the increased roughness, obtained by AFM, it is obvious the crystallization of this thin film sample. However, through XPS analysis, there can be seen that there were some contaminations at the surface, changing the VO_x form into V_6O_{13}. The samples didn't have any coating deposition or in-situ transfer to the XPS chamber to protect the easy oxidation of VO_2 into V_6O_{13}, at the surface [10], and this could have led to the results presented. At least, VO_2 (M) is present in bulk which is a positive indicator for the metal-to-insulator transition analysis.

3.2 Vanadium oxides produced by RF Magnetron Sputtering

Different sputtering depositions were performed varying the O_2 pressure in order to establish the optimal conditions for the formation of VO_2 monoclinic phase. The samples were annealed afterwards, at 400 ºC, 450 ºC and 500 ºC in the RTA system under N_2 atmosphere. D1

refers to the highest O_2 content deposition ($5x10^{-5}$ mbar), D2 to the medium O_2 content ($3x10^{-5}$ mbar) and D3 to the lowest O_2 content ($1x10^{-5}$ mbar).

3.2.1 X-Ray Diffraction (XRD)

All sputtered films were analyzed by XRD to determine the experimental conditions required to produce VO_2 monoclinic phase. In Figure 11 the diffractogram of all sputtered samples in order to see the differences between O_2 pressure used.

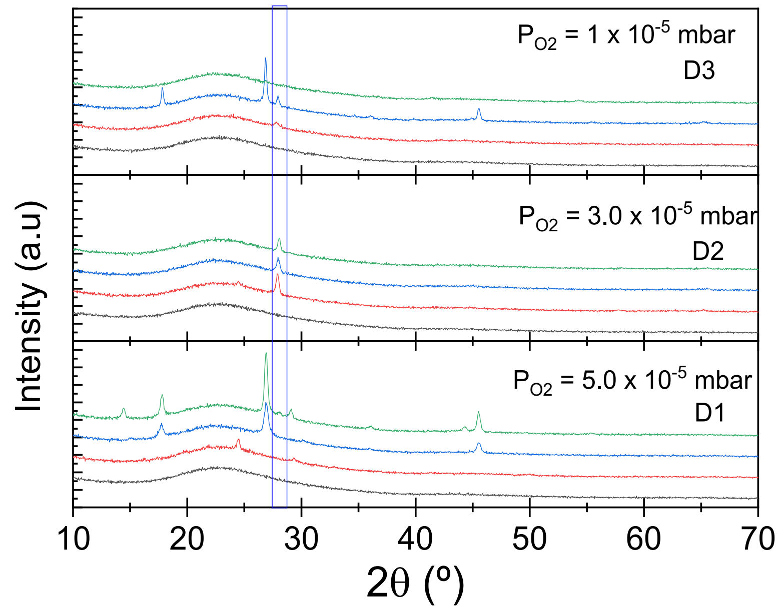

Figure 11 - XRD scans of all sputtered thin films

As seen, the VO_2 monoclinic peak (27.9º) is not very intense and only appears in some samples. To analyze this peak with closer attention, the samples were divided in groups of O_2 content used. Therefore, D1 group samples will be analyzed first, represented in Figure 12. This group corresponds to $5x10^{-5}$ mbar of O_2 pressure.

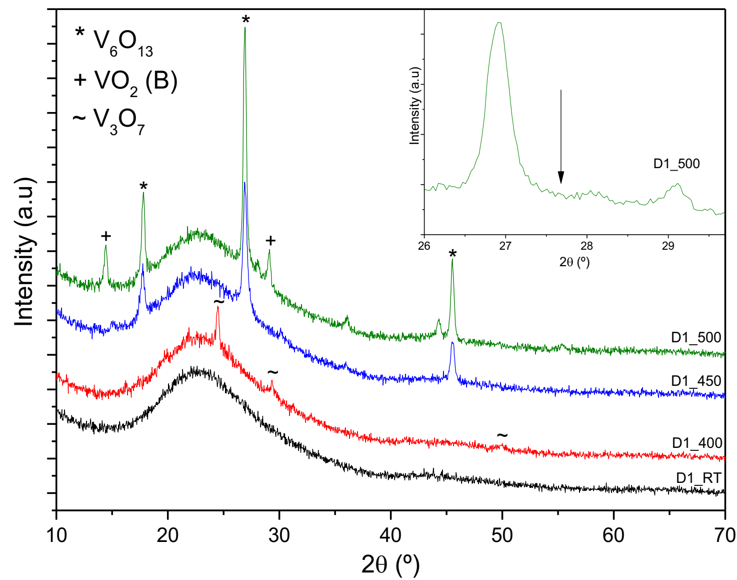

Figure 12 - XRD scans of D1 group samples

D1_RT, is amorphous and does not present any diffraction peaks and with increasing temperature, the crystallization of the films was obtained.

At D1_400, some peaks at 24.4º, 29.3º and 50.1º that may correspond to (600), (312) and (12 00) planes of V_3O_7 monoclinic phase C2/c (ISCD # 01-071-0454). This means there were some film crystallization but either RTA temperature was too low or O_2 pressure was too high to crystallize the desirable VO_2 monoclinic phase.

C_400 and C_500 present a new phase, having identical peaks with higher intensity for the sample C_500. These peaks are, at 2θ, 17.8º, 26.8º and 45.5º which agrees with the (002), (003) and (005) planes of V_6O_{13} monoclinic phase with space group C2/m (ISCD #01-075-1140).

Still, C_500 showed different peaks at 14.4º and 29.1º that relate to (001) and (002) planes of a VO_2 phase commonly found with space group C2/m (ISCD #01-081-2392). This phase, also nominated VO_2 (B), can be confused with the desirable one (VO_2(M)) since it is also a monoclinic structure. Although, it doesn't show a MIT transition and is mostly used in Li-on batteries as a cathode [13], [14]. On the inset Figure 12 a little ledge at 27.9º shown.

As said before, O_2 pressure could be too high or RTA temperature too low since the crystallization of VO_2 (M) phase wasn't clear.

Then, D2 group samples will be analyzed in Figure 13 were O_2 pressure used in the deposition was of $3x10^{-5}$ mbar.

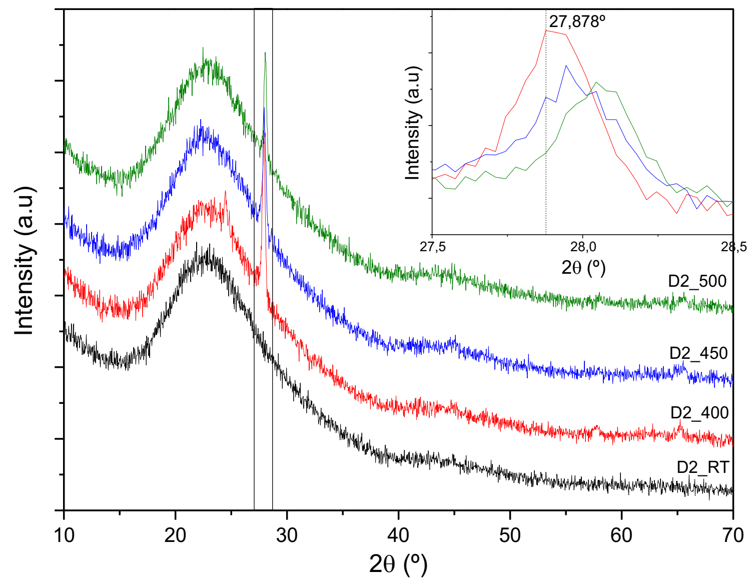

Figure 13 - XRD scans of D2 group samples

D2_RT, as D1_RT, showed amorphous behavior.

Samples from D2_400 to D2_500 shown one common peak around 27.9º which can be attributed to VO_2 (M) (ISCD #01-072-0514). On the inset Figure 13, as seen, D2_400 has a peak at 27.9º but the other samples shifted to the right of the peak. This suggests that the annealing temperature has an impact on the structural arrangement of the atoms in the films and might change the material into another phase of VO_2 other than VO_2 (M) or even another VO_x form.

Lastly, D3 group samples is represented in Figure 14 and O_2 pressure used was $1x10^{-5}$ mbar.

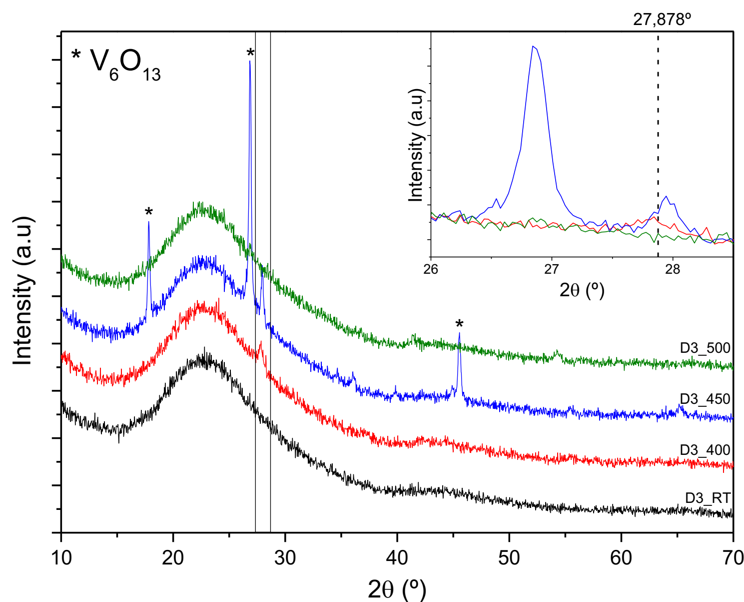

Figure 14 - XRD scans of D3 group samples

D3_RT was amorphous, as the other RT samples, even when the O_2 pressure changed.

At 400ºC, the crystallization of the film did not occur completely because it only showed a ledge around 27.9º. This can mean that the desirable phase is being formed but either RTA temperature wasn't high enough or the O_2 pressure was too low during the deposition of the films to allow the formation of VO_2 (M).

D3_450 diffractogram shows clear diffraction peaks and one of them is at 27.9º, which can be attributed to VO_2 (M) with space group P21/c (ISCD #01-072-0514). Additionally, other peaks (17.8º, 26.8º and 45.5º) correspond to V_6O_{13} (ISCD #01-075-1140), as seen before for D1_500.

In D3_500, no diffraction is shown indicating that this temperature may be too high to allow a stable crystalline phase. This is considered to be an unexpected result since at 500ºC, the crystallization should be clear into some form of a vanadium oxide.

As seen in the e-beam deposited films, only after RTA annealing at 500ºC VO_2 (M) was obtained. However, there was contaminations, at the surface, over-oxidizing the material changing it to V_6O_{13}.

In the sputtered films seen above, different pressures had different effects on the arrangement of the films. Of all samples, the one with VO_2 (M) in bulk was D2_400 which corresponds to $3x10^{-5}$ mbar of O_2 pressure and 400ºC of RTA temperature. V_6O_{13} was commonly found too since, according to *Mendialdua et al.*, VO_2 can over-oxidize easily into this VO_x form [10].

3.2.2 *X-ray Photoelectron Spectroscopy (XPS)*

The sputtered samples were also analyzed in groups according to O_2 pressure. It is important to remember that these samples were analyzed at the surface, by this technique.

Therefore, in Figure 15 a) D1 group samples are presented and the pressure used was $5x10^{-5}$ mbar. Figure 15 b) the oxidation state peaks are represented.

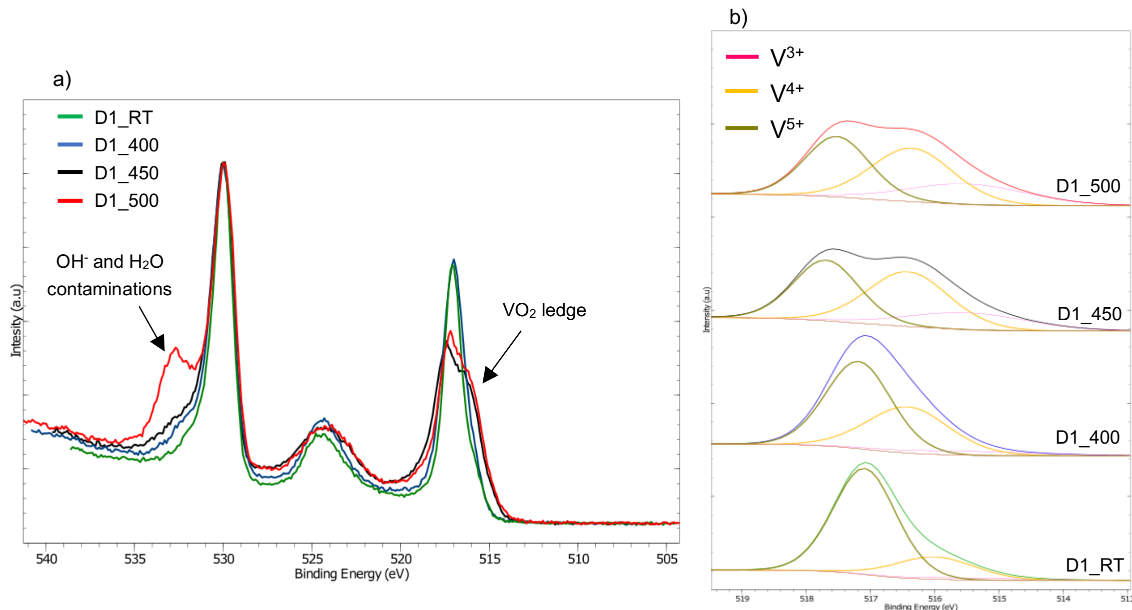

Figure 15 - XPS spectra of D1 group samples: a) all spectra; b) oxidation state peaks contributions

According to *Mendialdua et al.*, as said before, VO_2 can over-oxidize easily into V_6O_{13} or something similar, at the surface [10]. The state of oxidation V^{5+} can be from V_2O_5 or V_6O_{13} and

the difference between them is the narrower peaks that V_2O_5 presents which are the narrowest between the VO_x forms [10], [11] .

From Figure 15 a) D1_RT and D1_400 have an identical distribution. D1_RT has amorphous behavior as confirmed by XRD. D1_400 had oxidation occurring since V $2p_{1/2}$ peak seems to have a higher peak that the others. Also, in comparison to D1_RT and according to Table 5, the peaks widened (FWHM increased) which also contributes to confirm the oxidation at the surface to V_6O_{13}.

D1_450 and D1_500 had an abrupt decrease of V 2p peak height due to the increase of V^{4+} peak, as seen in **Erro! A origem da referência não foi encontrada.**Figure 15. These two samples relate to the desirable VO_x form which is VO_2. Although, these had contaminations in the surface, more intense at 500ºC. These contaminations can appear randomly since it is related to over-oxidation or only to exposure to air.

As the temperature increased, V^{3+} peak also increased but since its height was always lower than V^{4+} and V^{5+} peaks, this peak could have helped to widen the peaks and could be taking some height of V^{4+} peak. Although, this difference was not considered important since VO_2 was present.

In Table 5, it is represented the parameters extracted from *CasaXPS* to help the analysis.

Table 5 - XPS parameters of D1 group samples

Sample	**V^{4+}/ V^{5+}**	**V/O**	**$FWHM_{V^{4+}}$**	**$BE_{V^{4+}}$ (eV)**	**$FWHM_{V^{5+}}$**	**$BE_{V^{5+}}$ (eV)**
D1_RT	0.27	0.43	1.46	516.0	1.15	517.0
D1_400	0.66	0.43	1.50	516.2	1.20	517.0
D1_450	1.13	0.44	1.50	516.1	1.20	517.0
D1_500	1.11	0.46	1.50	516.0	1.20	517.0

Table 5 confirms the increased intensity from D1_450 and D1_500 since V^{4+}/V^{5+} ratio was superior to one. Although, the V/O ratio increased which means V 2p increased and it can be seen from Figure 15 that an increase in V 2p peaks relates to oxidations at the surface changing the structure to V_6O_{13}.

O_2 pressure of $3x10^{-5}$ mbar is represented in Figure 16 a) to see the differences in detail and in Figure 16 b), the peak state distribution is shown.

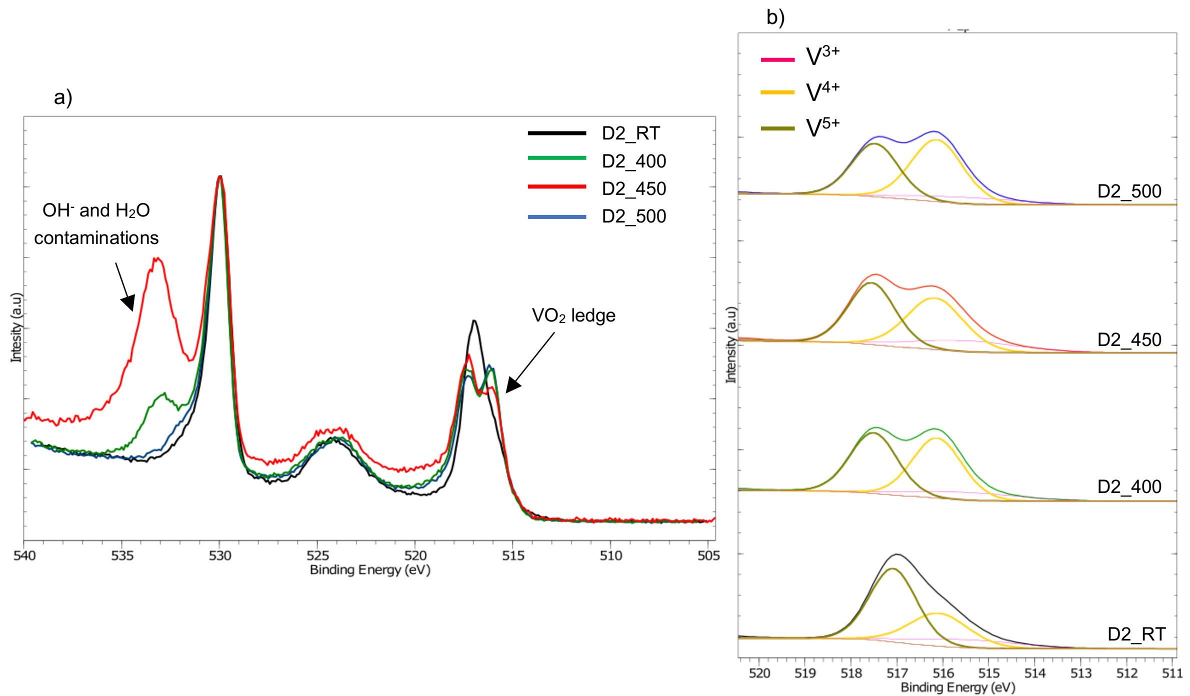

Figure 16 - XPS spectra of D2 group samples: a) all samples; b) oxidation state contributions

As seen before in D1_RT, D2_RT was amorphous. At 400°C, 450°C and 500ºC, the V 2p peak showed an abrupt change which was due to the rise of V^{4+} peak that showed a big difference between D2_RT and the other samples (Figure 16). This way, V^{4+} peak is revealing as V^{5+} is decreasing, which shows VO_2 is arising.

Concerning the O 1s peak, D2_400 and D2_450 have peaks confirming the contaminations at the surface. D2_400 had a contamination peak already visible but it didn't affect the VO_2 structure. At 450ºC, the intensity of the contamination peak increased which can be caused by over-oxidation. These contaminations, even at 450ºC, didn't affect the V^{4+} peak because, according to Table 6, a decrease of V/O ratio and V^{4+}/V^{5+} ratio above one means that VO_2 was present in the sample.

D2_500 presented no considerable contaminations in the O 1s peak and V^{4+}/V^{5+} ratio is the highest value between the four samples. Also, the V/O ratio increased, and this shows some possible oxidation. This samples also relates to VO_2. In Figure 16 b), a little V^{3+} peak appears but did not affect the samples since its height was always lower than V^{4+} and V^{5+} peaks.

Table 6 - XPS parameters of D2 group samples

Sample	V^{4+}/V^{5+}	V/O	$FWHM_{V^{4+}}$	$BE_{V^{4+}}$ (eV)	$FWHM_{V^{5+}}$	$BE_{V^{5+}}$ (eV)
D2_RT	0.56	0.41	1.50	516.1	1.20	517.1
D2_400	1.05	0.38	1.27	516.1	1.20	517.5
D2_450	1.01	0.25	1.45	516.2	1.20	517.5
D2_500	1.29	0.45	1.33	516.1	1.20	517.5

At last, in Figure 17 the O_2 pressure is $1x10^{-5}$ mbar which is the D3 group samples and oxidation state contributions are shown.

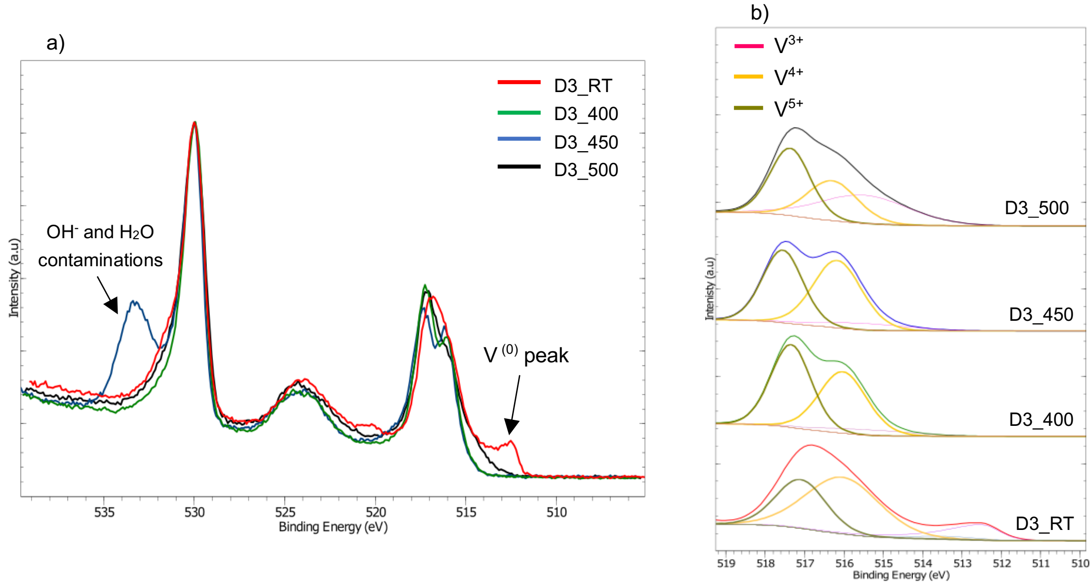

Figure 17 - XPS spectra of D3 group samples: a) all spectra; b) oxidation state contributions

In this set, D3_RT showed a $V^{(0)}$ peak at 512.5 eV. This means that D3 contains metallic V since it was not subjected to the RTA treatment. Also, the O_2 pressure was smaller in comparison to the other samples which could be insufficient for the crystallization of the films and, therefore, a metallization of the surface was reached. Also, according to Table 7, the V^{4+} and V^{5+} peaks widen ($FWHM_V{}^{4+}$ and $FWHM_V{}^{5+}$ are 2.20 eV and 1.50 eV, respectively) and V/O ratio is the highest of D3 samples. $V^{(0)}$ peak can have influence in this since it is located to the right of these peaks and as long as this peak increases, the V 2p peak can be broadened.

D3_400 and D3_500 showed a decrease in V^{4+}/V^{5+} ratio which means VO_2 changed its structure one more time due to over-oxidation.

V^{3+} peak is only visible at 500ºC since is not a considerable peak at the other samples. In D3_500, the peak had still a lower height compared with V^{4+} and V^{5+} but could be taking some percentage out of V4+ and adding this to the over-oxidation, VO_2 is no longer present.

In Table 7, the important values of the samples extracted from *CasaXPS* are represented.

Table 7 - XPS parameters of D3 group samples

Sample	V^{4+}/V^{5+}	V/O	$FWHM_{V^{4+}}$	$BE_{V^{4+}}$ (eV)	$FWHM_{V^{5+}}$	$BE_{V^{5+}}$ (eV)
D3_RT	1.71	0.52	2.20	516.0	1.50	517.1
D3_400	0.88	0.45	1.42	516.0	1.20	517.3
D3_450	1.12	0.27	1.45	516.2	1.20	517.6
D3_500	0.74	0.45	1.50	516.3	1.20	517.4

From O 1s peak (Figure 17 a)), D3_450 has a contamination peak but it wasn't significant to change the structure of VO_2 since V^{4+}/V^{5+} ratio is higher than one, meaning V^{4+} peak has higher content than V^{5+} peak.

D3_500 showed no considerable contaminations but the sample over oxidized since the V^{4+} peak is wider than D3_400 and there is an increase in the V 2p peaks. This sample also relates to V_6O_{13}.

From XPS analysis, the optimal conditions are determined looking for the higher ratio of V^{4+}/V^{5+}. However, V/O ratio is also important since over-oxidation can occur at the surface. The sample believed to have the most VO_2 phase, taking these parameters in consideration, is D2_500 (3x10-5 mbar of O_2 pressure and 500ºC of RTA temperature) since the V^{4+}/V^{5+} ratio is 1.29 and V/O ratio is 0.45. This means that V^{4+} exists in more abundance and the oxidation at the surface is not significant.

3.2.3 Atomic Force Microscopy (AFM)

AFM technique was used to characterize the roughness and crystallization of the films. Here, four samples of the same deposition at different RTA temperatures will be displayed in order to identify the crystallization differences as RTA temperature increases.

Then, one sample from each O_2 pressure will be chosen to see the changes with different pressures. The remaining samples will be in Annex for reference.

Figure 18 shows the D1 group samples (5x10^{-5} mbar) analyzed with Atomic Force Microscope and in Table 8, the values for RMS roughness and maximum peak height are displayed.

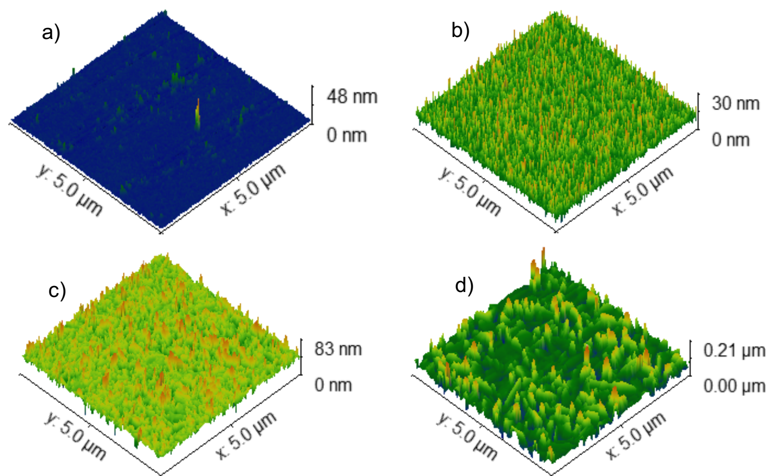

Figure 18 - AFM 3D representation of D1 group sample surfaces: a) D1_RT; b) D1_400; c) D1_450; d) D1_500

Table 8 - Structural parameters extracted from AFM for D1 group samples

Sample	RMS Roughness, Sq (nm)	Median peak height (nm)
D1_RT	1.1889	4.3790
D1_400	2.5262	11.692
D1_450	6.5855	43.525
D1_500	26.169	70.342

As seen in the figure and table above, the roughness of the films is increasing as RTA temperature increases. This means that bigger temperatures cause higher crystallization of the surface and is directly proportional to the roughness. The median peak height also increases as RTA temperature increases which proves that the crystallization of the peaks is clearer when RTA

temperature is higher. At the temperature of 500ºC, there is an abrupt increase at the parameters, mostly in the roughness of these surfaces, since it adds 20 nm.

Figure 19 shows the group of samples in whose RTA temperature is 450ºC. This was the chosen RTA temperature since VO_2 (M) phase is present in all of them and the crystallization of the films is clearer by the imagens. Table 9 displays the parameters analyzed and, as said before, the remaining samples are in Annex.

As a reminder, D1 corresponds to $5x10^{-5}$ mbar, D2 to $3x10^{-5}$ mbar and D3 to $1x10^{-5}$ mbar.

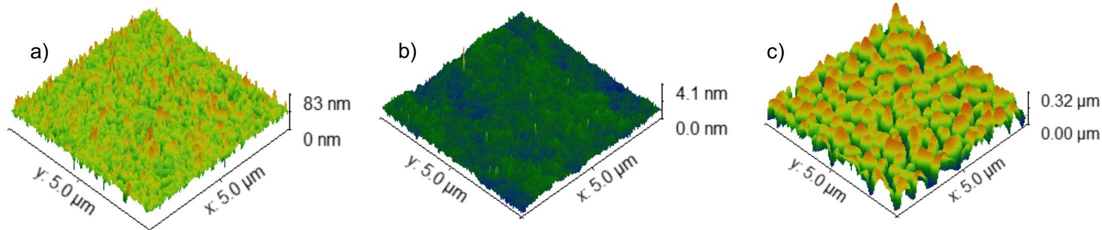

Figure 19 - AFM 3D representation of the samples annealed at 450ºC

Table 9 - Structural parameters extracted from AFM for the samples annealed at 450ºC

Sample	**RMS Roughness, Sq (nm)**	**Median peak height (nm)**
D1_450	6.5855	43.525
D2_450	46.632	110.24
D3_450	57.957	183.46

From Figure 19, it's clear the height of the peaks is increasing as O_2 pressure decreases. In Table 9, it is also evident that the roughness of the films is increasing, which means that with less O_2 pressure in the chamber, the crystallization of the peaks is enhanced.

At this phase, the optimal conditions were determined. By XRD, the best conditions were $3x10^{-5}$ mbar of O_2 pressure and 400ºC of annealing temperature, and by XPS the O_2 pressure was the same, but RTA temperature was 500ºC. This way, the O_2 pressure used was $3x10^{-5}$ mbar since it was common to both analyses. The RTA temperature chosen was 450ºC since it was between 400ºC and 500ºC, where VO_2 also appears in both analysis and therefore, the transition could appear as well.

As temperature increases, the crystallization of the thin films becomes clearer and an increase of over-oxidation at the surface is more visible. This over-oxidation normally changes the material from VO_2 (M) to V_6O_{13} [10].

3.3 In-situ measurements in MIM VO_2 devices

After optimizing the deposition conditions for VO_2 monoclinic phase, MIM devices were produced on ITO coated glasses. For such, VO_2 thin films were deposited by sputtering using the optimized condition: $3x10^{-5}$ mbar of O_2 pressure and RTA at 450 ºC under N_2 atmosphere.

In-situ measurements were performed by means of XRD and XPS where the structure and chemical composition of the films were studied under temperature ramps.

3.3.1 XRD in-situ

In order to confirm the MIT transition, a deposition of VO_2 thin films in a silicon substrate was made under 250 mbar of N_2 environment. In Figure 20, an in-situ XRD with temperature ramps was performed. The temperatures went from 50ºC to 100ºC. This was made in order to analyze the existence of the metal-to-insulator transition.

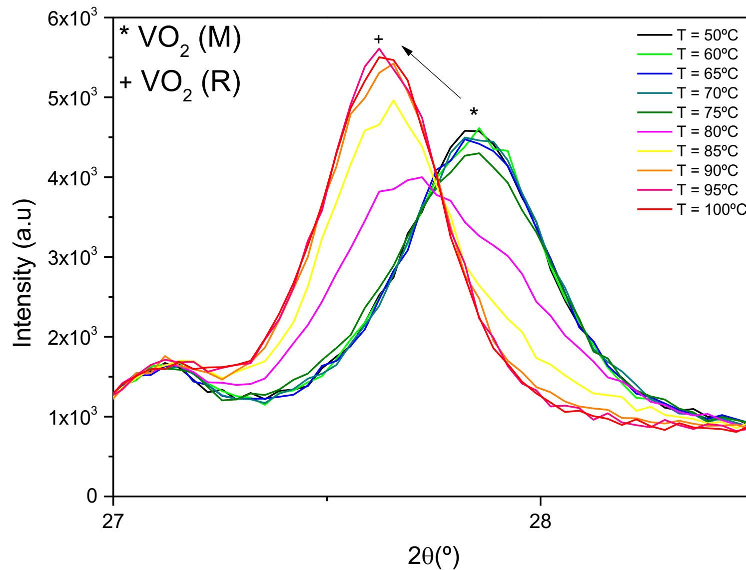

Figure 20 - XRD scans of VO_2 thin films with temperature ramps

The transition of VO_2 is represented in Figure 20 since it can be seen the change in the peak when the temperature increases. This shows the phase of this VO_x form since it can go from VO_2 (M) to VO_2 (R). However, the MIT transition for VO_2 (M) is said to be around ~68ºC and in this case, it started after this temperature (75ºC). This can mean that the substrate used for this measure had an influence in the temperature transition changing it to higher temperatures or there is a heat dissipation through the substrate.

This experiment means that the optimal condition found to obtain VO_2 thin films is correct, being these conditions: $3x10^{-5}$ mbar of O_2 pressure and 450ºC of RTA temperature.

To obtain the confirmation of the reversible transition, the same experiment with a cooling temperature from 100ºC to 50ºC should be done. In addition, the substrate for this measure should be corning glass instead of silicon since the temperature transition was not the desired one and to have the same substrate during all investigation.

3.3.2 In-situ heating experiments in the XPS chamber

XPS in-situ measurements were made to see the differences according to temperature changes. Since there is a metal-to-insulator (MIT) at ~68ºC, samples were submitted to temperatures below and above this transition. The temperatures used were RT, 45ºC, 60ºC, 75ºC and 90ºC. There were also measurements one and four days after the first measurements to see

any changes due to the UHV conditions and exposure to x-rays. The sample was kept inside the chamber in vacuum all times.

The first measurements made are represented in Figure 21. These started at RT and increased until 90ºC. In this analysis, in Figure 21 b) there are represented the contributions of the oxidation state peaks. This time, V^{3+} peak was not found and therefore it is not represented from now on.

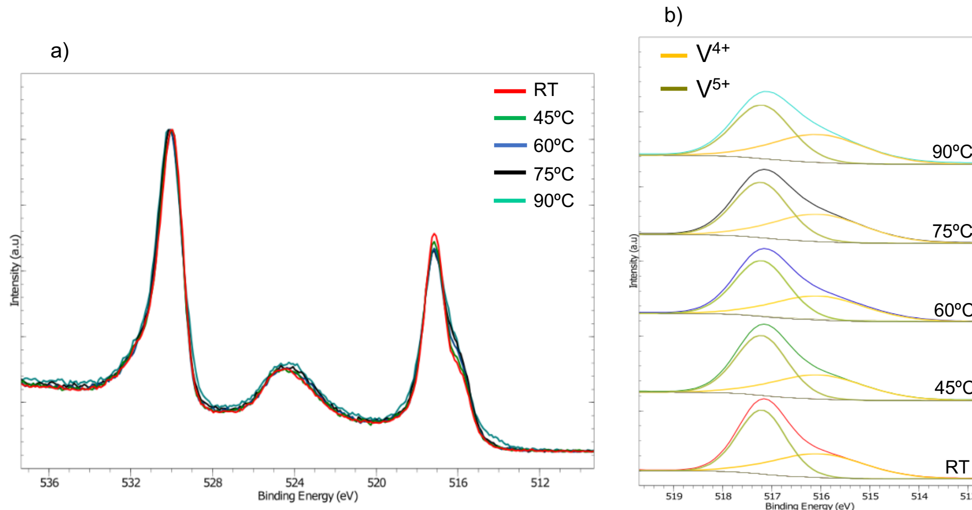

Figure 21 - XRD spectra of optimized VO_2 thin films with increasing temperature: a) all spectra; b) oxidation state contributions

From these spectra, there were no visible peaks of contaminations, looking at O 1s peak. Although, according to the increase of V 2p ½ peak, there was some oxidation at the surface. Since V/O ratio represented in Table 10 did not change significantly as temperature increased, the sample could have over-oxidize before entering the XPS chamber.

Table 10 - XPS parameters of optimized VO_2 thin films with increasing temperature

XPS T (ºC)	V^{4+}/ V^{5+}	V/O	$FWHM_{V^{4+}}$	$BE_{V^{4+}}$ (eV)	$FWHM_{V^{5+}}$	$BE_{V^{5+}}$ (eV)
RT	0.71	0.46	2.20	516.0	1.15	517.2
45	0.72	0.46	2.20	516.0	1.24	517.2
60	0.74	0.47	2.20	516.0	1.29	517.2
75	0.83	0.47	2.20	516.0	1.31	517.2
90	0.83	0.49	2.20	516.0	1.39	517.2

At V $2p_{3/2}$ peak, as temperature rises, the V^{4+} peaks increases and V^{5+} decreases as also confirmed by an increase of V^{4+}/V^{5+} ratio from Table 10. However, this ratio suggests that V^{5+} peak is still higher than V^{4+} which means that VO_2 in no longer present, at the surface. This can mean that before entering the XPS chamber, an over-oxidation had already changed the surface sample into V_6O_{13}.

In Figure 22, there is a representation of valence band of this sample in order to confirm the semiconductor to metal transition. This transition, according to *Wertheim et al.,* provides an opening gap at the Fermi energy (E_F=0 eV) since at room temperature VO_2 presents a semiconductor behavior [23]. As temperature increases and above the transition temperature,

this gap should be occupied and an increase of the density of states at the Fermi level should be seen [23].

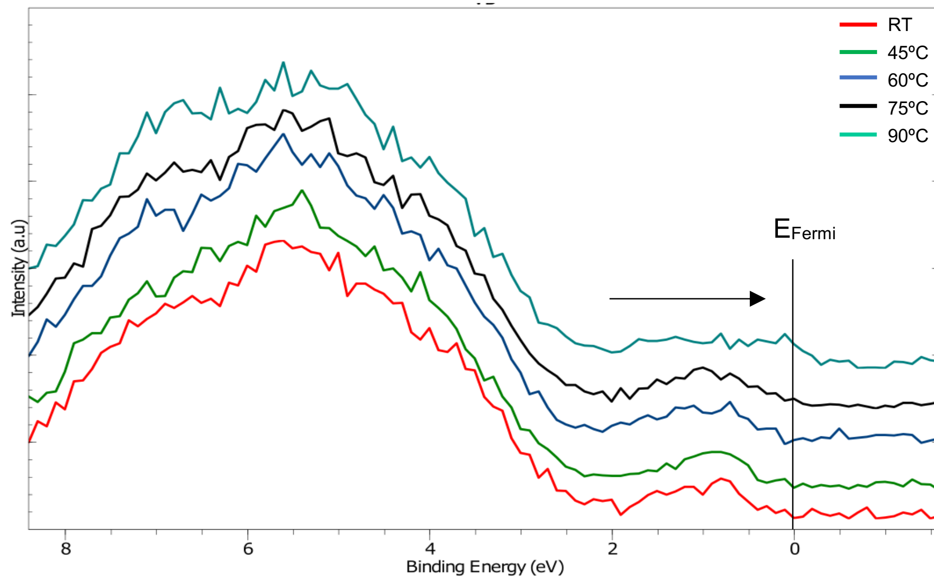

Figure 22 - Representation of VO2 thin films valence band with increased temperature

As seen in the figure above, at temperatures below the MIT transition (RT, 45ºC and 60ºC) the band structure stays until the Fermi level suggesting a semiconductor behavior. At temperatures above the transition, mostly at 90ºC, the structure is starting to go over the Fermi level, suggesting the transition to a metal state. The temperature at which the transition occurs corroborates with the heating ramp conducted in the XRD.

Figure 23, shows spectra one day after the first measurements, with the same temperature used but this time, starting at 90ºC until RT.

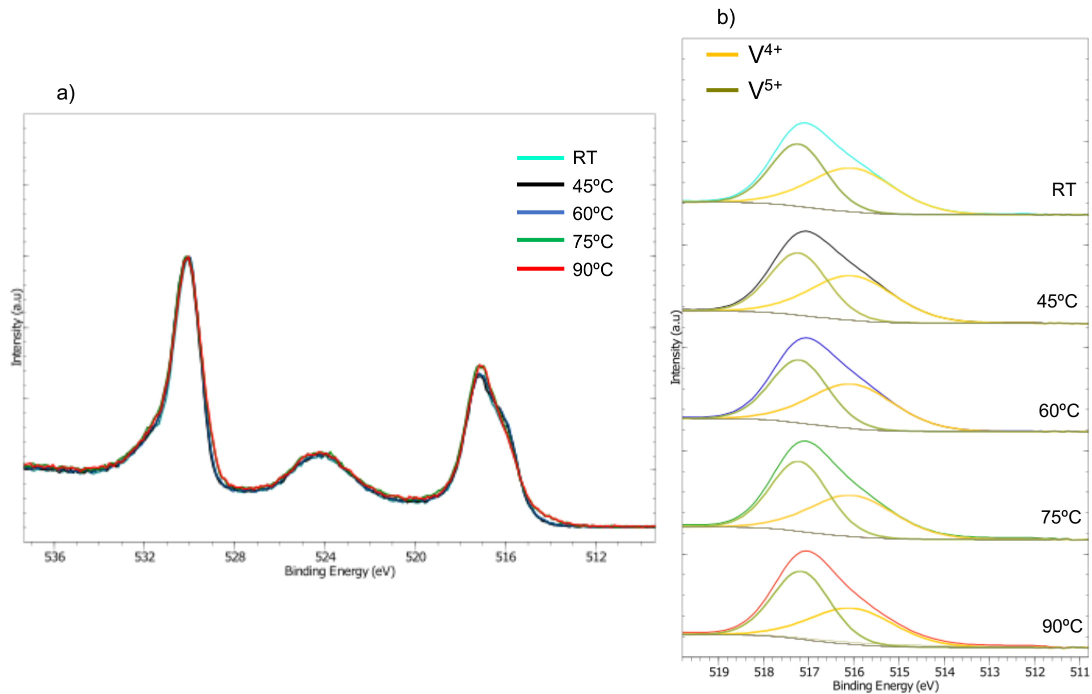

Figure 23 - XRD spectrum of optimized VO2 thin films with decreasing temperature: a) all spectra; b) oxidation state contributions

In comparison with Figure 21, the spectra represented in Figure 23 shows a higher V^{4+} peak.

Looking at the figure above, V^{5+} peak seems higher than V^{4+} peak which can mean that the over-oxidation at the surface was still present even though the sample was kept at the chamber for one day. To confirm this assumption, Table 11 in presented below.

Table 11 - XPS parameters of VO_2 thin films with decreased temperature

XPS T (ºC)	V^{4+}/ V^{5+}	V/O	$FWHM_{V^{4+}}$	$BE_{V^{4+}}$ (eV)	$FWHM_{V^{5+}}$	$BE_{V^{5+}}$ (eV)
90	0.79	0.46	2.20	516.0	1.49	517.2
75	0.87	0.49	2.20	516.0	1.50	517.2
60	1.04	0.50	2.20	516.0	1.50	517.2
45	1.05	0.50	2.20	516.0	1.50	517.2
RT	1.07	0.49	2.20	516.0	1.44	517.2

Here, the temperature started at 90ºC and decreased until it reached room temperature. Looking at Table 11, V^{4+}/V^{5+} was increasing as temperature was decreasing. As the sample was kept in the XPS chamber, in a vacuum condition and subjected to x-rays all times, the surface sample might have reduced to the bulk configuration which is VO_2 after the transition from metal to semiconductor. The ratio V/O did not change much and so, the reduction could have occurred during the measurement.

In order to see the transition in more detail, the valence band region of the VO_2 thin film when temperature is decreasing, is shown in Figure 24.

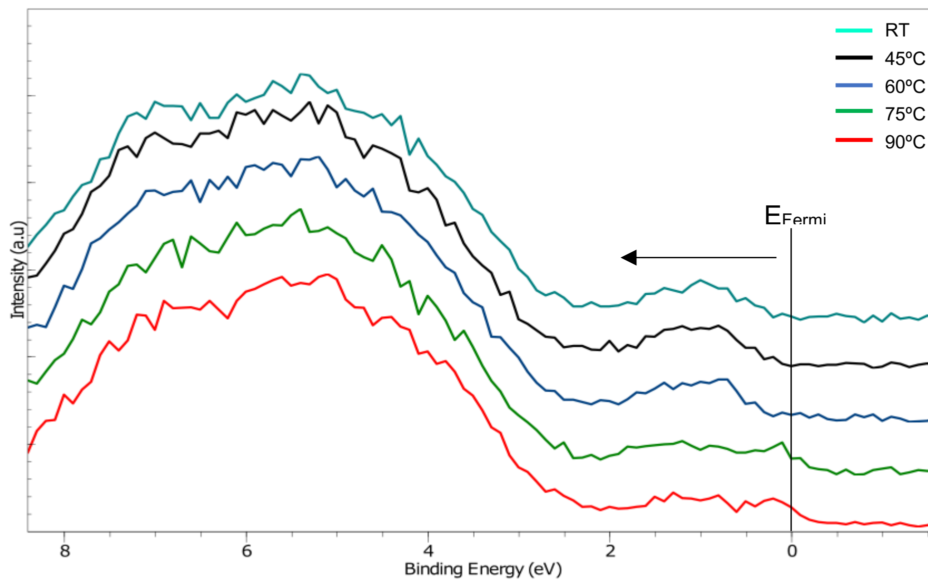

Figure 24 - Representation of VO_2 thin film valence band with decreased temperature

A Fermi edge at 0 eV, at temperatures of 75ºC and 90ºC, is clearly visible which relates to the metallic state of VO_2. At temperatures below the transition the Fermi edge disappears and the valence band maximum of the semiconducting VO_2 becomes visible, again. Note that the transition now occurs below 75ºC, confirming that the change in observed transition temperature is related to whether heating or cooling is performed. This way, the reversibility of VO_2 metal-to-insulator transition is showed [23].

Furthermore, the sample was kept in the chamber for four more days. This was made to verify the importance of a vacuum condition since it tends to oxidize, at the surface, changing the structure of the sample.

In Figure 25, XPS spectrum of the VO_2 thin film kept at RT with different dates of analysis being one day after the first analysis and four days after.

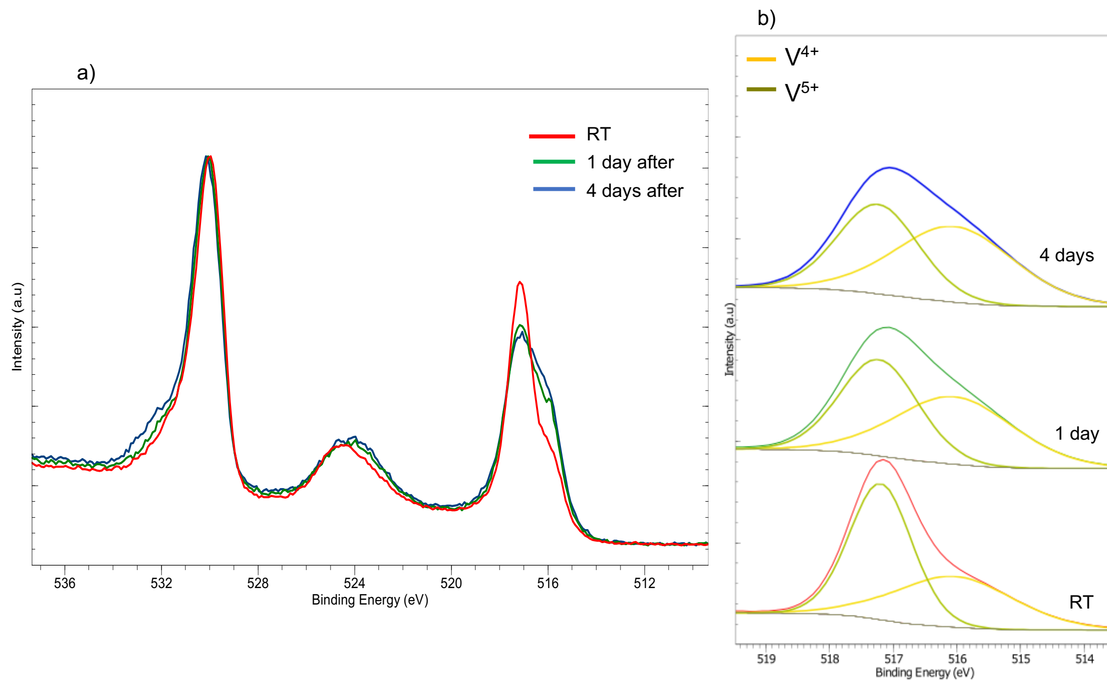

Figure 25 - XPS spectrum of VO_2 thin film kept in the vacuum chamber for four days: a) all spectra; b) oxidation state contributions

The surface of the sample could have reduced due to the vacuum conditions under exposure of x-rays and the thermal energy provided by the temperature ramps. However, there is still a considerable amount of V^{5+} present at the surface (Figure 25), meaning that to obtain a pure VO_2 state, an in-situ transfer between the deposition chamber and measurement chambers should be taken in consideration. This is in order to protect the thin films from contaminations and over-oxidation at the surface. These would facilitate the analysis of the samples and the application of the desirable phase and structure of VO_2.

3.3.3 Electrical Characterization of MIM devices

MIM devices were produced by sputtering using shadow masks with circular metal contacts of Molybdenum of 1 mm wide diameter on the VO_2 films. In Figure 26, there is an IV curve at RT with a potential sweep from -1V to 1V to see the behavior of the device and to obtain the resistance and resistivity values.

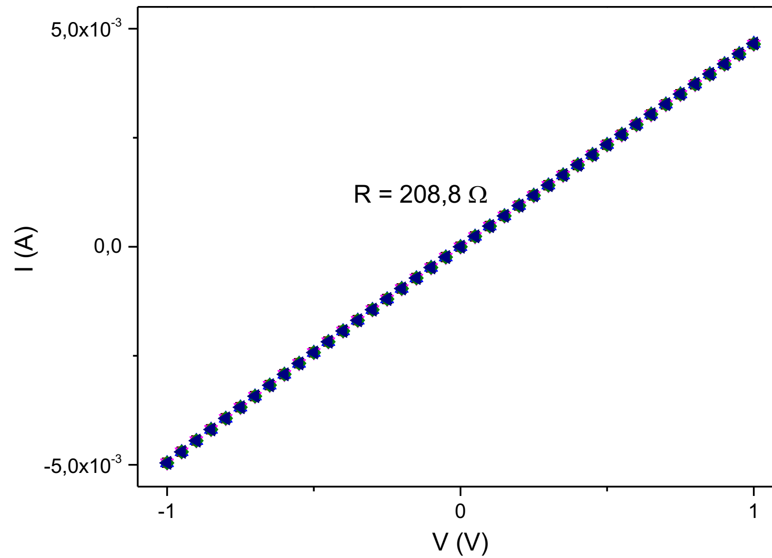

Figure 26 - Electrical characterization of VO2 thin film MIM devices

As seen, the IV curve is ohmic, and the resistance value can be extracted as the inverse of the slope and the resistivity knowing the area of the contact. The contact had 1 mm of wide diameter and the thin film 200 nm of thickness.

$$R = \rho \times \frac{L_{\text{thin film}}}{A_{\text{contact}}} \leftrightarrow \rho = R \times \frac{A_{\text{contact}}}{L_{\text{thin film}}} = 208.8 \times \frac{\pi\left(\frac{1 \times 10^{-3}}{2}\right)^2}{200 \times 10^{-9}} = 820.0\ \Omega\ \text{m} = 8.2\ \Omega\ \text{cm}$$

This value is higher than the usual since, at RT, the usual value of resistance rounds 10^{-3} Ω cm for single-crystalline substrates [6].

These devices were then electrically characterized with a potential sweep from -0.5 V to 0.5 V in order to obtain the electrical resistance of the films at different temperatures. The heating of the sample was carried by a heating stage of Agilent. In this case only the heating of the sample was carried but the cooling should also be done in order to evaluate the reversibility of the transition.

In Figure 27, there are the IV curves when heating the sample from RT to 100ºC. The resistance was extracted and expressed by a R vs T graphic in Figure 28 in order to confirm the resistance changes as temperature increases.

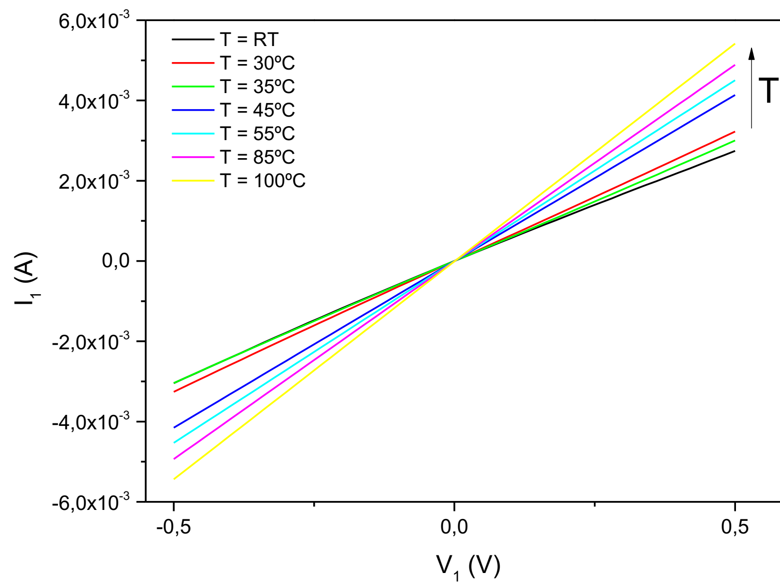

Figure 27 - Electrical characterization of VO2 thin film MIM devices with increased temperature

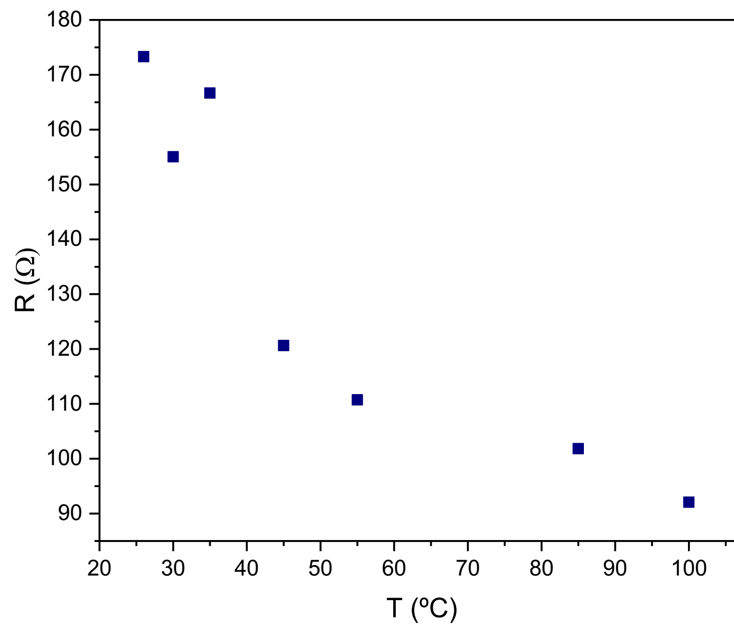

Figure 28 - Resistance evolution of VO2 thin film MIM devices with increased temperature

As seen, as temperatures rises, the resistance values decrease from a first value of 173.3 Ω to 92.2 Ω and this decrease of resistance with the increasing temperature is typical of a semiconductive behavior. According Yang et al., the transition change from a high resistance state to a low resistance state which can mean the VO_2 structure changed from monoclinic to tetragonal rutile, according to the transition at 68ºC [6].

Measuring in MIM devices, the low thickness of the films may have led to an electrical driven transition occurring at lower temperatures. This data is still inconclusive.

To confirm the reversibility of this transition, the same IV curves should be obtained during the cooling of the sample with the same temperature ramps. Also, the resistance should be obtained in order to see the change from a low resistance to a high resistance state.

4. Conclusion and Future Perspectives

The main goal of this work was to determine the experimental conditions in order to obtain the reversible metal-to-insulator transition at ~68ºC of VO_2 monoclinic phase.

As a starting point, VO_x thin films were deposited by e-beam evaporation followed by an annealing treatment at different temperatures (300ºC, 400ºC, 450ºC, 500ºC) and the characteristic peak of VO_2 monoclinic phase, at ~27ºC, was found for 500ºC of RTA temperature. Also, an abrupt increase on the crystallization and roughness of the thin film presented by AFM clarified that this temperature was the optimal condition for e-beam depositions. From XPS analysis, it was confirmed that due to long exposures to air or OH^- and water contaminations, the surface can over-oxidize and change its VO_x form, as it happened. So, VO_2 (M) was presented in the bulk and V_6O_{13} was at the surface of these samples.

Rf-sputtering was also meant to optimize and so, some depositions with different O_2 pressures ($1x10^{-5}$ mbar, $3x10^{-5}$ mbar, $5x10^{-5}$ mbar) were performed. These were followed by RTA treatment at different temperatures (400ºC, 450ºC, 500ºC), as well. By means of XRD, it was concluded that different O_2 pressure generate different VO_x forms. The one where VO_2 (M) was most clearly observed relates to $3x10^{-5}$ mbar of O_2 pressure and 400ºC of annealing temperature. XPS analysis agreed with the O_2 pressure but the RTA temperature more suited was 500ºC. This was due to the V^{4+}/V^{5+} ratio and V/O ratio where the V^{4+} peak (VO_2) was found in more abundance and with less contaminations and over-oxidations, at the surface. Therefore, the optimal conditions chosen to produce VO_2 thin films by sputtering were with $3x10^{-5}$ mbar of O_2 pressure and 450ºC of RTA treatment. By AFM the crystallization of the peaks for this condition was 46.632 nm and the median peak height was 110.24 nm which can confirm the increased crystallization and roughness of the thin films.

MIM devices were fabricated using sputtering circular contacts of Molybdenum with the optimal condition. By the analysis, the metal-to-insulator transition was achieved between 60ºC and 75ºC since there is a shift of the VB of the samples that confirms the change from metal to semiconductor and vice-versa. The reversibility of this transition was demonstrated by XPS.

From an electrical characterization with increased temperature, resistance changes were obtained. At RT, the resistance was 173.3 Ω and at 100ºC was 92.2 Ω. This behavior is expected for a semiconductor and from this preliminary data it is not possible to confirm the transition.

In the future, to avoid the contaminations and over-oxidation of the surface, an in-situ transfer from the deposition chamber to the analyses chamber or a protective coating of thin films should be considered. This coating shouldn't affect the thin film properties. Also, a more detailed in-situ analysis with temperature ramps should be carried to tune in the specific temperature of this transition.

Since this material is supposed to work as an electrical switch, a much better electrical characterization should be performed in order to evaluate the capacity of this device to work as a memristor. To work as a memristor, the capacity to store information is not only essential but also the speed of this transition that is said to be ultrafast (picoseconds) [3]–[7]. Therefore, a resistance-switching phenomenon in MIM devices with resistance states (with cooling temperatures), resistance hysteresis with temperature ramps, speed, state retention, are some of the electrical characterization that can be done.

Some other characterization techniques such as AFM or even an optical characterization with temperature ramps can be interesting to see changes in structural and optical properties.

VO_2 can be a starting point to discover other vanadium oxides that can work as a switch since some of them also have the transition, although, at higher temperatures. Furthermore, this transition temperature can be changed by doping, lattice mismatch, controlling grain size, among others [24].

A holder developed in the CENIMAT laboratories can also be used in XRD, or other techniques if it fits, to heat the sample with lower intervals of temperature ramps or even, heating or cooling the sample while measuring the properties at the same time [21].

5. Bibliography

[1] C. A. Mack, “FiftyYears of Moore ’ s Law,” *IEEE Fellow*, vol. 24, no. 2, p. 2008, 2011.
[2] D. B. Strukov, G. S. Snider, D. R. Stewart, and R. S. Williams, “The missing memristor found,” *Nature*, vol. 453, no. 7191, pp. 80–83, 2008.
[3] Y. Zhou, Z. Yang, and S. Ramanathan, “Multi-Resistance States Through Electrically Driven Phase Transitions in VO2/HfO2/VO2 Heterostructures on Silicon,” *Ieee Electron Device Lett.*, vol. 33, no. 1, pp. 101–103, 2012.
[4] N. Bahlawane and D. Lenoble, “Vanadium oxide compounds: Structure, properties, and growth from the gas phase,” *Chem. Vap. Depos.*, vol. 20, no. 7–9, pp. 299–311, 2014.
[5] P. Markov, R. E. Marvel, H. J. Conley, K. J. Miller, R. F. Haglund, and S. M. Weiss, “Optically Monitored Electrical Switching in VO2,” *ACS Photonics*, vol. 2, no. 8, pp. 1175–1182, 2015.
[6] Z. Yang, C. Ko, and S. Ramanathan, “Oxide Electronics Utilizing Ultrafast Metal-Insulator Transitions,” *Annu. Rev. Mater. Res.*, vol. 41, no. 1, pp. 337–367, 2011.
[7] Z. Yang, C. Ko, and S. Ramanathan, “Metal-insulator transition characteristics of VO2 thin films grown on Ge(100) single crystals,” *J. Appl. Phys.*, vol. 108, pp. 1–6, 2010.
[8] Q. Lu *et al.*, “Electrochemically Triggered Metal–Insulator Transition between VO2 and V2O5,” *Adv. Funct. Mater.*, vol. 28, no. 34, pp. 1–8, 2018.
[9] S. Surnev, M. G. Ramsey, and F. P. Netzer, “Vanadium oxide surface studies,” *Prog. Surf. Sci.*, vol. 73, no. 4–8, pp. 117–165, 2003.
[10] J. Mendialdua, R. Casanova, and Y. Barbaux, “XPS studies of V2O5, V6O13, VO2 and V2O3,” *J. Electron Spectros. Relat. Phenomena*, vol. 71, no. 3, pp. 249–261, 1995.
[11] G. Silversmit, D. Depla, H. Poelman, G. B. Marin, and R. De Gryse, “Determination of the V2p XPS binding energies for different vanadium oxidation states (V5+ to V0+),” *J. Electron Spectros. Relat. Phenomena*, vol. 135, no. 2–3, pp. 167–175, 2004.
[12] E. Hryha, E. Rutqvist, and L. Nyborg, “Stoichiometric vanadium oxides studied by XPS,” *Surf. Interface Anal.*, vol. 44, no. 8, pp. 1022–1025, 2012.
[13] Y. Zhang, “VO2(B) conversion to VO2(A) and VO2(M) and their oxidation resistance and optical switching properties,” *Mater. Sci. Pol.*, vol. 34, no. 1, pp. 169–176, 2016.
[14] C. Wu and Y. Xie, “Promising vanadium oxide and hydroxide nanostructures: From energy storage to energy saving,” *Energy Environ. Sci.*, vol. 3, no. 9, pp. 1191–1206, 2010.
[15] W. Hong *et al.*, “Theoretical investigation of vanadium oxide film with surface microstructure,” *Opt. Appl.*, vol. 47, no. 4, pp. 601–609, 2017.
[16] F. A. Chudnovskii and G. B. Stefanovich, “Metal-insulator transition in disordered VO2,” *J. Solid State Chem.*, vol. 98, no. 1, pp. 137–143, 1992.
[17] Z. Shao, X. Cao, H. Luo, and P. Jin, “Recent progress in the phase-transition mechanism and modulation of vanadium dioxide materials,” *NPG Asia Mater.*, pp. 581–605, 2018.
[18] T. Driscoll, H. T. Kim, B. G. Chae, M. Di Ventra, and D. N. Basov, “Phase-transition driven memristive system,” *Appl. Phys. Lett.*, vol. 95, no. 4, pp. 2–5, 2009.
[19] R. Schmitt, J. Spring, R. Korobko, and J. L. M. Rupp, “Design of Oxygen Vacancy Configuration for Memristive Systems,” *ACS Nano*, vol. 11, no. 9, pp. 8881–8891, 2017.
[20] O. Applicata, “Theoretical investigation of vanadium oxide film with surface microstructure,” vol. XLVII, no. 4, 2017.
[21] M. S. Farto, “Multipurpose XRD holder for the simultaneously characterization of the structural and electrical properties of vanadium oxides.”
[22] M. C. Biesinger, L. W. M. Lau, A. R. Gerson, and R. S. C. Smart, “Resolving surface chemical states in XPS analysis of first row transition metals, oxides and hydroxides: Sc, Ti, V, Cu and Zn,” *Appl. Surf. Sci.*, vol. 257, no. 3, pp. 887–898, 2010.
[23] G. K. Wertheim, M. Campagna, H. J. Guggenheim, J. P. Remeika, and D. N. E. Buchanan, “X-ray photoemission study of metal-insulator transitions in VO2, V2O3 and NiS,” vol. 235, pp. 235–237, 2008.
[24] S. H. Bae *et al.*, “The memristive properties of a single VO2 nanowire with switching controlled by self-heating,” *Adv. Mater.*, vol. 25, pp. 5098–5103, 2013.

6. Annexes

Annex A – AFM measurements

AFM measurements of all D2 and D3 group samples are represented in Figure 29 and in Figure 30. Also, the values for RMS roughness and Median peak height are displayed in Table 12 and in Table 13.

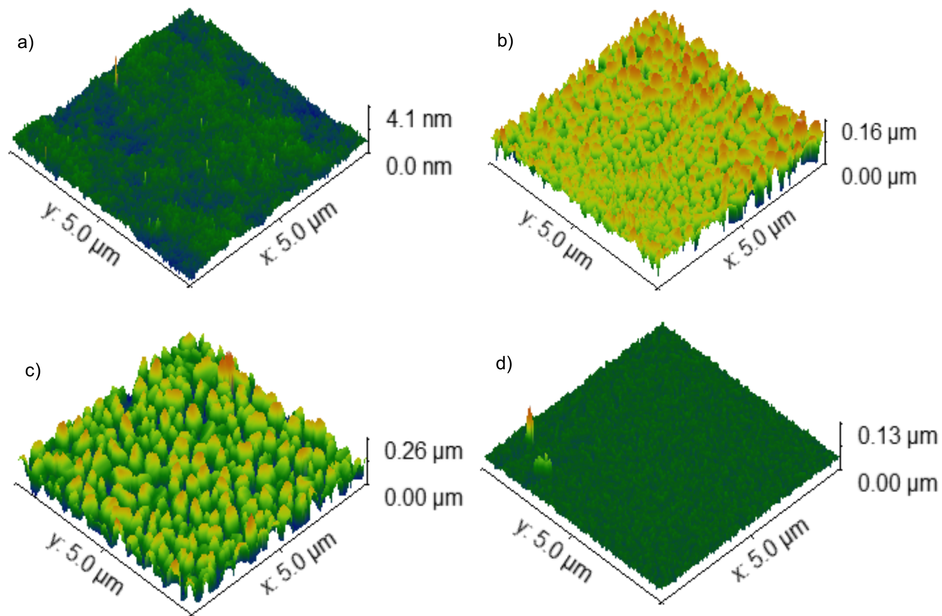

Figure 29 - AFM 3D representations of D2 group samples: a) D2_RT; b) D2_400; c) D2_450; d) D2_500

Table 12 - Structural parameters extracted from AFM for the D2 group samples

Sample	RMS Roughness, Sq (nm)	Median peak height (nm)
D2_RT	0.19917	0.92291
D2_400	23.258	90.130
D2_450	46.632	110.24
D2_500	4.7549	34.772

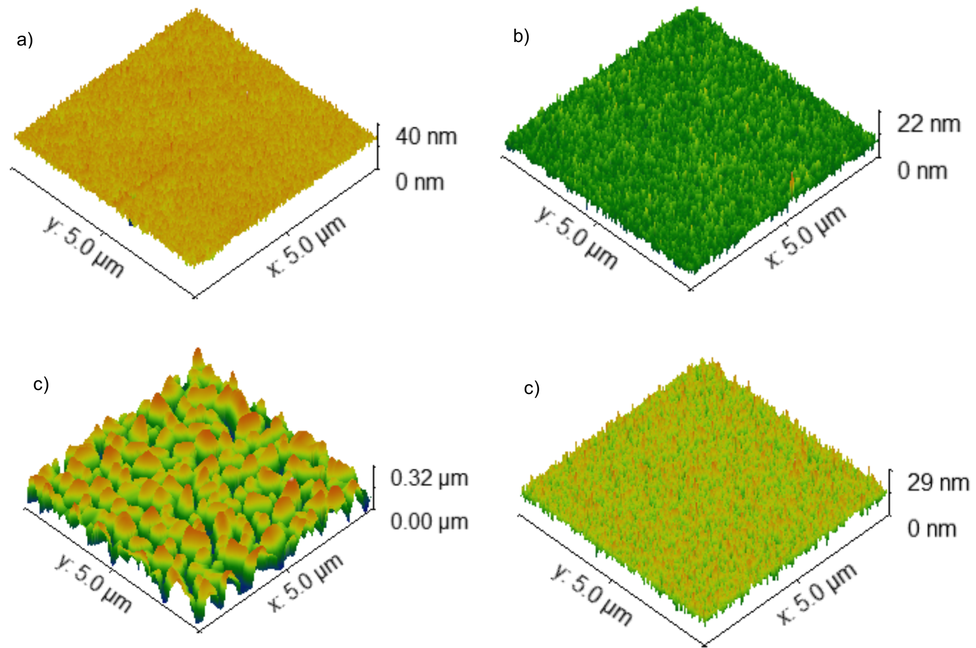

Figure 30 - AFM 3D representations of D3 group samples: a) D3_RT; b) D3_400; c) D3_450; d) D3_500

Table 13 - Structural parameters extracted from AFM for the D3 group samples

Sample	**RMS Roughness, Sq (nm)**	**Median peak height (nm)**
D3_RT	1.8501	10.558
D3_400	1.4989	7.9158
D3_450	57.957	183.46
D3_500	2.9362	12.198

Annex B – Thin films resistors designs

150 um

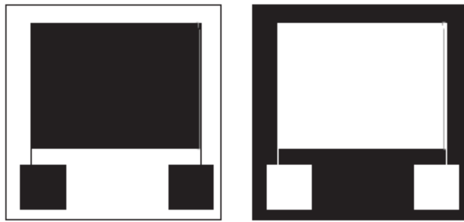

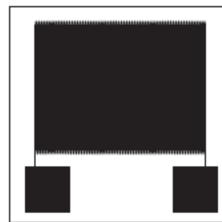

300 um

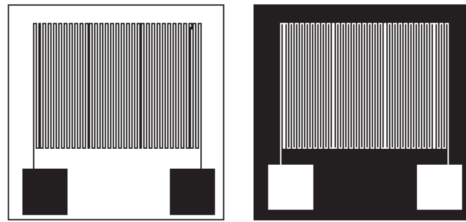

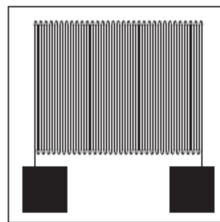

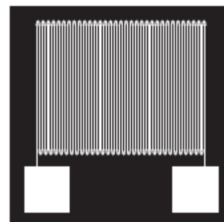

200 um

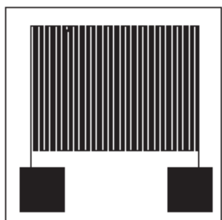

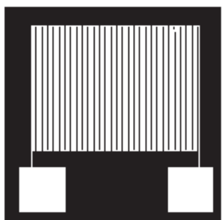

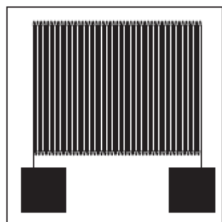

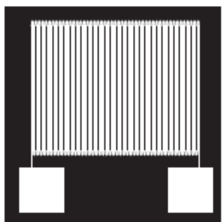

400 um

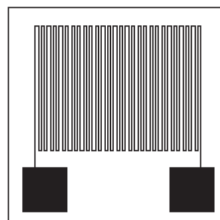

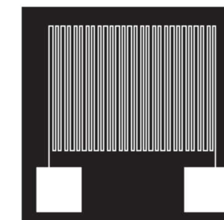

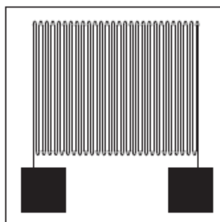

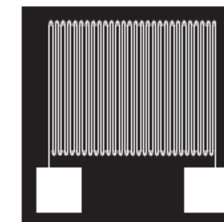

Figure 31 - Thin films resistor designs with different width between stripes

Annex C – ITO characterization with thin film resistors

As already mentioned in Materials and Methods, a design of resistor thin films was made and four different designs with two different geometries (round or straight edges) were created and presented in the Figure 31.

Photolith masks for etching and lift off were produced. The idea was to produce heating elements on the backside of the device substrate, to allow a controllable heating of the sample while performing the mentioned characterization. This way, instead of analyzing the response of the devices on different heating stages, as the ones existent on each characterization tool, the sample can be heated "in-situ" while characterized and always keeping the same temperature profile.

The masks produced were tested in previous work on Au (Silver) films (by lift-off) and ITO films (wet etching). Unfortunately, only the ITO resistors were successfully produced. The etching was performed using a HCl-$FeCl_3$ solution.

These resistive elements were electrically tested with a potential sweep from -5V to 5V and increased temperature until 100ºC and is represented in Figure 32.

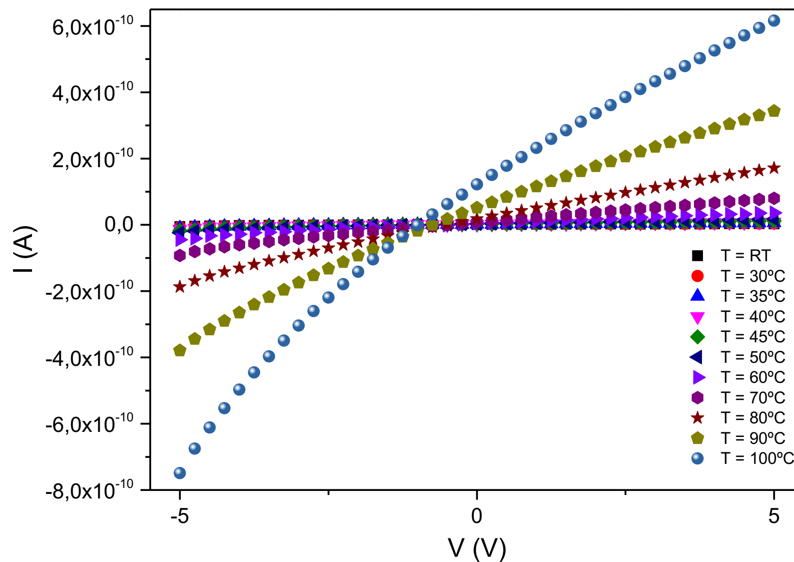

Figure 32 - IV curves representation of a test using a resistor design as a possible heating element

As temperatures rises, once more, the resistance of the device decreases, and the value can reach MΩ. These can be due the geometry of the design such as the long path and the short width (W = 400 µm).

The next step would be to optimize the resistor thin films designs in order to decrease the resistance value. Also, the use of the holder fabricated in CENIMAT|i3n would be interesting to perform a morphological, optical and electrical characterization simultaneously with temperature ramps.